The EMBO Journal (2010) 29, 1176–1191 | © 2010 European Molecular Biology Organization | All Rights Reserved 0261-4189/10
www.embojournal.org

THE EMBO JOURNAL

A polycystin-2 (TRPP2) dimerization domain essential for the function of heteromeric polycystin complexes

Aurélie Giamarchi[1,8], Shuang Feng[2,8], Lise Rodat-Despoix[1,8], Yaoxian Xu[2], Ekaterina Bubenshchikova[3], Linda J Newby[2], Jizhe Hao[1], Christelle Gaudioso[1], Marcel Crest[1], Andrei N Lupas[4], Eric Honoré[5], Michael P Williamson[6], Tomoko Obara[3,7], Albert CM Ong[2,*] and Patrick Delmas[1,*]

[1]Centre de Recherche en Neurophysiologie et Neurobiologie de Marseille, UMR 6231, CNRS, Université de la Méditerranée, Bd Pierre Dramard, Marseille Cedex 15, France, [2]Kidney Genetics Group, Academic Unit of Nephrology, The Henry Wellcome Laboratories for Medical Research, University of Sheffield Medical School, Sheffield, UK, [3]Department of Medicine, MetroHealth Medical Center, Case Western Reserve University, MetroHealth Drive, Cleveland, OH, USA, [4]Department of Protein Evolution at the Max-Planck-Institute for Developmental Biology, Tuebingen, Germany, [5]IPMC-CNRS UMR 6097, route des Lucioles, Valbonne, France, [6]Department of Molecular Biology and Biotechnology, University of Sheffield, Sheffield, UK and [7]Department of Genetics, Case Western Reserve University, Cleveland, OH, USA

Autosomal dominant polycystic kidney disease (ADPKD) is caused by mutations in two genes, *PKD1* and *PKD2*, which encode polycystin-1 (PC1) and polycystin-2 (PC2), respectively. Earlier work has shown that PC1 and PC2 assemble into a polycystin complex implicated in kidney morphogenesis. PC2 also assembles into homomers of uncertain functional significance. However, little is known about the molecular mechanisms that direct polycystin complex assembly and specify its functions. We have identified a coiled coil in the C-terminus of PC2 that functions as a homodimerization domain essential for PC1 binding but not for its self-oligomerization. Dimerization-defective PC2 mutants were unable to reconstitute PC1/PC2 complexes either at the plasma membrane (PM) or at PM-endoplasmic reticulum (ER) junctions but could still function as ER Ca^{2+}-release channels. Expression of dimerization-defective PC2 mutants in zebrafish resulted in a cystic phenotype but had lesser effects on organ laterality. We conclude that C-terminal dimerization of PC2 specifies the formation of polycystin complexes but not formation of ER-localized PC2 channels. Mutations that affect PC2 C-terminal homo- and heteromerization are the likely molecular basis of cyst formation in ADPKD.

The EMBO Journal (2010) **29,** 1176–1191. doi:10.1038/emboj.2010.18; Published online 18 February 2010
Subject Categories: membranes & transport; molecular biology of disease
Keywords: ion channel-signalling complex; polycystic kidney disease; polycystin-1; polycystin-2; TRP channel

Introduction

Autosomal dominant polycystic kidney disease (ADPKD) is among the most common life-threatening inherited human diseases worldwide. The primary phenotype of ADPKD is the progressive development in both kidneys of multiple fluid-filled cysts, which eventually result in end-stage renal failure (Gabow, 1990; Calvet and Grantham, 2001; Ong and Harris, 2005). Mutations in two causative genes, *PKD1* and *PKD2*, encoding polycystin-1 (PC1) and polycystin-2 (PC2), respectively, can initiate cyst formation after homozygous loss-of-function mutations (Mochizuki *et al*, 1996; Harris, 1999; Wu and Somlo, 2000).

PC1 is a 4302 amino-acid membrane protein with 11 transmembrane spans, a large N-terminal extracellular region containing a number of adhesive domains and an intracellular C-terminal region of ~225 amino acids (Hughes *et al*, 1995; Sandford *et al*, 1997). On the basis of its predicted structure and functional features, PC1 is postulated to be a plasma membrane (PM) receptor involved in cell–cell/matrix interaction and the regulation of several signalling pathways linked to cell proliferation (Arnould *et al*, 1998; Kim *et al*, 1999; Bhunia *et al*, 2002; Parnell *et al*, 2002; Delmas *et al*, 2002a; Streets *et al*, 2009). PC2, also called TRPP2, is smaller (968 amino acids) with six transmembrane spans, a pore forming region, and cytoplasmic N- and C-terminal tails. By virtue of its structural homology, PC2 belongs to the transient receptor potential (TRP) superfamily of ion channels, which broadly function as cellular sensors for multiple stimuli (Mochizuki *et al*, 1996; Giamarchi *et al*, 2006; Damann *et al*, 2008).

PC1 and PC2 interact physically (Qian *et al*, 1997; Tsiokas *et al*, 1997; Newby *et al*, 2002) and form a Ca^{2+}-permeable non-selective cation channel when expressed heterologously (Hanaoka *et al*, 2000; Delmas, 2004; Delmas *et al*, 2004). Both proteins co-localize in the primary cilia of epithelial kidney cells where they are hypothesized to promote mechanosensation and contribute to fluid-flow sensation (Nauli *et al*, 2003; Praetorius and Spring, 2003). At variance, in the case of pressure sensing by arterial myocytes, PC2 rather inhibits mechanosensitivity (Sharif-Naeini *et al*, 2009).

Besides its localization in the primary cilium, PC2 is present in the endoplasmic reticulum (ER), the PM, the

*Corresponding authors. P Delmas, Centre de Recherche en Neurophysiologie et Neurobiologie de Marseille, UMR 6231, CNRS, Université de la Méditerranée, CS80011, Bd Pierre Dramard, 13344 Marseille Cedex 15, France. Tel.: +33 4 91 69 89 78; Fax: +33 4 91 69 89 77; E-mail: patrick.delmas@univmed.fr or ACM Ong, Kidney Genetics Group, Academic Unit of Nephrology, The Henry Wellcome Laboratories for Medical Research, University of Sheffield Medical School, Beech Hill Road, Sheffield S10 2RX, UK. Tel.: +44 114 271 3402; Fax: +44 114 271 1711; E-mail: a.ong@sheffield.ac.uk
[8]These authors contributed equally to this work

Received: 8 December 2009; accepted: 25 January 2010; published online: 18 February 2010

adherens junctions and the basolateral cell surface of kidney epithelial cells (Cai *et al*, 1999; Foggensteiner *et al*, 2000; Koulen *et al*, 2002; Scheffers *et al*, 2002; Yoder *et al*, 2002; Luo *et al*, 2003; Roitbak *et al*, 2005; Fu *et al*, 2008). PC2 can function as an ER-located Ca^{2+}-release channel in some systems and has been shown to interact directly with several ER-resident proteins, including the inositol 1,4,5 triphosphate receptor ($InsP_3Rs$) (Li *et al*, 2005) and syntaxin 5 (Geng *et al*, 2008). Among other PC2-interacting proteins described so far, α-actinin, fibrocystin and diaphanous-related formin 1 protein (mDia1) have been shown to regulate PC2 channel activity (Li *et al*, 2006; Wu *et al*, 2006; Bai *et al*, 2008b). Recent data also provided compelling evidence that PC2 heteromerizes with TRPC1 (Tsiokas *et al*, 1999; Bai *et al*, 2008a; Zhang *et al*, 2009) and TRPV4 (Köttgen *et al*, 2008) to form channels with distinct properties from homomers. PC2 has also been shown to be expressed in mouse embryonic nodal cells, in the absence of PC1, where it is implicated in the determination of left-to-right asymmetry (Pennekamp *et al*, 2002; McGrath *et al*, 2003, Karcher *et al*, 2005). Overall, these observations show that PC2 exerts PC1-dependent as well as -independent functions and raise the question as to the mechanisms that direct assembly of PC2 into homomeric and heteromeric complexes.

The C-terminal region of PC2 contains residues important for PC2 function (Celic *et al*, 2008). A newly identified coiled-coil domain located in the C-terminus of PC2 has been proposed to mediate assembly of PC2 into a homotrimer (Yu *et al*, 2009). This result was rather unexpected given that a variety of structural and functional studies has shown that TRP channels assemble as tetramers (Tsuruda *et al*, 2006). Recent evidence using atomic force microscopy directly contradicts the conclusion by Yu *et al* (2009), by showing that the PC2 homomer assembles as a homotetramer (Kobori *et al*, 2009).

To address these discrepancies, we have performed further biochemical and functional characterization of the newly identified PC2 C-terminal coiled-coil domain. Our results reveal that this domain mediates dimerization of the C-terminus of PC2 and recognition of PC1. Selective disruption of this dimerization domain abrogated functions of heteromeric PC1/PC2 but not homomeric PC2 ion channel complexes, both *in vitro* and *in vivo*. The specificity of this interaction is therefore a key regulatory step in the formation of PC1/PC2 ion channel complexes. Mutations that disrupt PC1/PC2 interactions either by preventing the C-terminal dimerization of PC2 or its heterodimerization with PC1 lead to cyst formation.

Results

Identification of an evolutionarily conserved coiled-coil domain in the C-terminal region of PC2

The current model of the C-terminus of PC2 (CT2) consists of an EF-hand motif overlapping with a short putative coiled-coil (CC) domain and a long α-helix spanning F839–R919 (Mochizuki *et al*, 1996; Qian *et al*, 1997; Tsiokas *et al*, 1997; Celic *et al*, 2008) (Figure 1A). Using the coiled-coil prediction algorithm PCOILS (Lupas *et al*, 1991), we identified two stretches of residues E769–L796 (CC1) and S835–A873 (CC2) with elevated CC probabilities. However, only the S835–A873 motif exhibited a strong probability (~1) of coiled-coil formation and is very well preserved on a representative subset of PC2 orthologs (Figure 1B).

A similar analysis of other members of the PKD and TRP families indicates that only PKD2L1 (TRPP3) possesses a comparable C-terminal coiled coil at a conserved location in the primary sequence (Figure 1B). Display of the S835–A873 sequence on a coiled-coil helical wheel diagram shows that the predicted 'a' and 'd' core positions correspond predominantly to hydrophobic residues (Figure 1C). The CC2 region was further modelled in Figure 1D using BeammotifCC, with the first residue of the model S835 set to position 'd' of the first heptad repeat. The model suggests that CC2 participates in a parallel two-stranded structure with strong potential for dimerization (Figure 1D).

Dimerization of the C-terminal of PC2 is mediated by CC2 using Y2H

We first asked whether the putative CC2 could function as an autonomous assembly domain using the yeast two-hybrid system (Y2H). Y2H assays were performed using the C-terminus (CT2, aa680–968) of PC2 or its truncations to delineate the minimal interacting regions for homodimerization (Figure 2A). Truncation of CT2 to E871 (680–871) showed a stronger interaction with full-length CT2, activating ADE2 reporter. This is compatible with an inhibitory domain in the distal half of CT2 (872–968) and/or a conformational change induced by deletion of the distal sequence (see NMR spectra). The minimal interacting region for CT2 self-association was 833–871 (Figure 2A). Consistent with this, the peptide 680–798, which includes CC1 but excludes CC2, was unable to interact with CT2. Furthermore, disruption of CC2 by mutations of key hydrophobic residues (V846, I853, I860 and L867; we will call this mutant CT2-4M) to alanine abolished CT2/CT2 interaction. In contrast, missense changes in CT2 at R807Q (likely polymorphism) (Rossetti *et al*, 2007) and S812A (a CK2 phosphorylation site) (Köttgen and Walz, 2005) had little effect on CT2/CT2 binding. These data clearly indicate that CC2 undergoes self-oligomerization.

Mutations of CC2 hydrophobic residues abolish CT2/CT2 interaction

We generated CT2 bacterial fusion proteins using different epitope tags to assay for the ability of CC2 to directly mediate homophilic interactions in GST pull-down assays. As shown in Supplementary Figure 1A, a minimal region of GST-(799–871), which excludes CC1 but includes CC2, could bind to Thio-CT2 with affinity equal to GST-CT2. For unknown reasons, we could not purify GST-(833–871) from bacterial lysates using glutathione beads so this region could not be tested. Nevertheless, the introduction of CC2 mutations into Thio-CT2 (CT2-4M) completely abolished its ability to bind to GST-(799–871) and GST-CT2 (Supplementary Figure 1A). In addition, we substituted the hydrophobic residue M849 in full-length PC2 with the hydrophilic residue proline, and assessed the mutational effect on its interaction with CD8-CT2. CD8-CT2 immunoprecipitated wild-type PC2 but failed to immunoprecipitate PC2-M849P and PC2-4M (Supplementary Figure 1B). Similarly, a CD8-CT2 deletion mutant (CD8-679–824), lacking CC2, could no longer bind to full-length PC2 (Supplementary Figure 1B). Conversely, wild-type PC2 immunoprecipitated CT2 but not CT2-4M (data not shown).

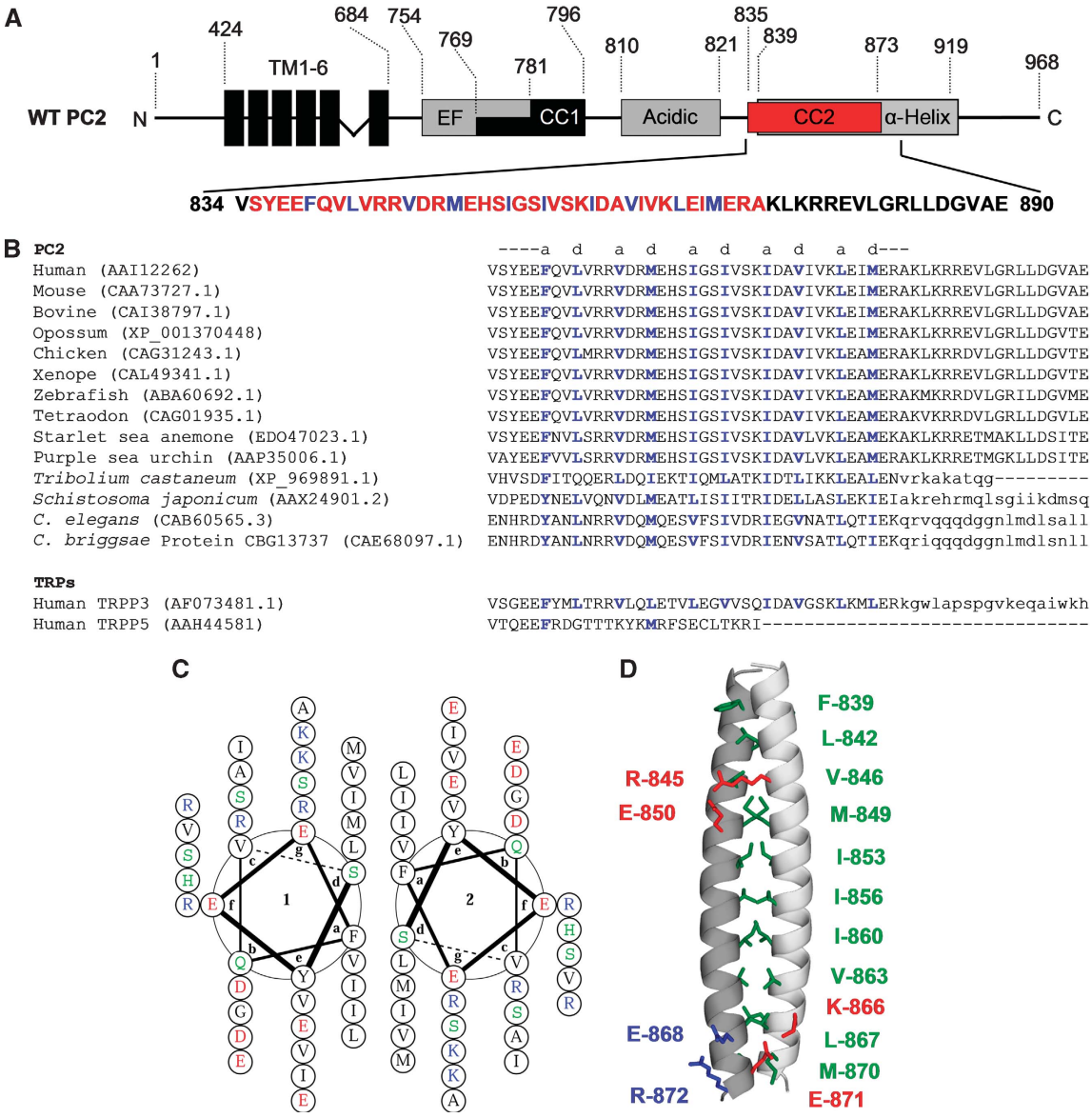

Figure 1 In silico model of PC2 coiled-coil region. (**A**) Schematic structure of hPC2. The previously reported EF-hand, CC1, acidic cluster and α-helix are indicated. Our proposed coiled coil (CC2) and its sequence are shown in red, with the 'a' and 'd' residues predicted by PCOILS highlighted in blue. (**B**) Alignment of conserved coiled coils in PC2 orthologs (top) and PKD family members (bottom). 'a' and 'd' positions are indicated. (**C**) Helical wheel projection of CC2 (S835–A873). Coiled-coil positions a–g are indicated. Amino acids are coloured: hydrophobic, black; basic, blue; acidic, red; and polar, green. Note that hydrophilic residues at the interface of the coiled coil make oligomerization favourable. (**D**) Side chains of the amino acids involved in the dimeric CC2 interactions. The model is shown in side view with the N-terminus at the bottom. Core residues 'a' and 'd' of each heptad repeat are in green, intra- and intermolecular salt bridges are in red and blue, respectively.

CT2 behaves primarily as a dimer in solution by analytical ultracentrifugation

To further examine the oligomeric structure of CT2, we performed analytical ultracentrifugation analysis of His-CT2 and His-CT2-4M by sedimentation velocity at concentrations between 0.3 and 0.6 mg/ml. The results for both proteins at 0.6 mg/ml are plotted in Figure 2B as the distribution of sedimentation coefficients. For His-CT2, the major component sedimented between 4 and 5 s with a $s_{20,w}$ (concentration-average corrected for water at 20°C) of 4.32 s. In contrast, the major component for His-CT2-4M sedimented around 2 s with a corresponding $s_{20,w}$ of 1.86 s.

His-CT2 protein was then analysed by sedimentation equilibrium to measure the protein molecular masses in solution. Equilibrium at 18 000 rpm was only established in cells where the protein concentration exceeded 0.3 mg/ml. Absorbance (A280 nm) and interference data from three scans (0.4–0.6 mg/ml) were analysed using different parts of the curves. The molecular weight of the major peak for His-CT2 was estimated as a single species at 69.9 kDa. As the calculated molecular weight of His-CT2 is 35 kDa, this species likely represents CT2 dimers. A small broad peak (0.25 molar ratio; 166.6 ± 21.2 kDa) was also noted. These two peaks likely correspond to the 4.32 s (major) and 9 s (minor) peaks seen by sedimentation velocity (left panel in Figure 2B). The best fit to the data was obtained from a model predicting a major dimer species with a minor peak of higher MW material (contaminants and a possible tetramer).

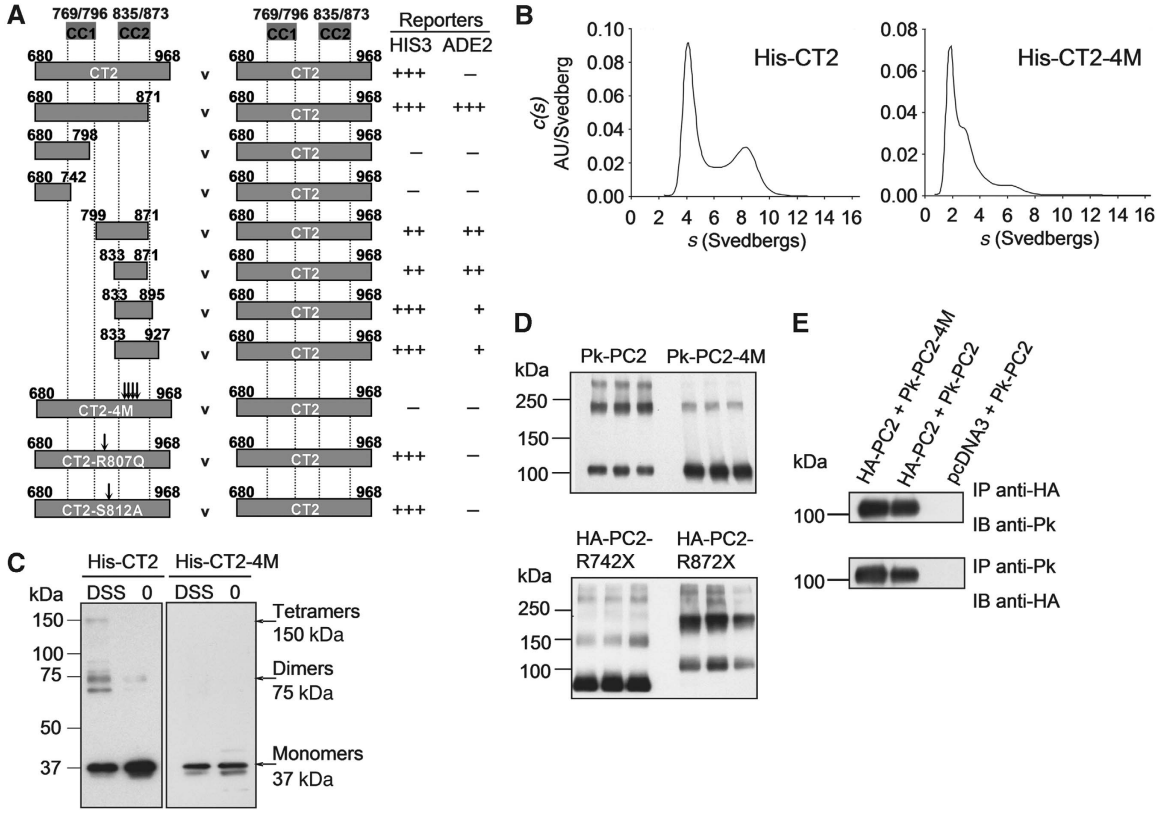

Figure 2 The coiled-coil domain CC2 is critical for self-oligomerization of the C-terminus of PC2. (**A**) Directed yeast two-hybrid assays using full-length CT2 (680–968) to investigate self-association. CT2 truncations containing or deleting two predicted coiled-coil regions, CC1 (769–796) and CC2 (833–873) were used as baits to refine the minimal interacting sequence. Site-specific mutations in CC2 (CT2-4M: V846A, I853A, I860A, L867A) but not two other changes (R807Q, S812A), disrupted this interaction. Coiled-coil domains are indicated. (**B**) Analytical ultracentrifugation (AUC) analysis of His-CT2 and His-CT2-4M by sedimentation velocity plotted as the distribution of sedimentation coefficients (s). Absorbance (275 nm) data for 0.6 mg/ml samples are shown. The major peak for His-CT2 sediments around 4 s, whereas that for His-CT2-4M sediments around 2 s. The MW of the major His-CT2 peak was measured as 69.9 kDa by sedimentation equilibrium. (**C**) Cross-linking assays of His-CT2 and His-CT2-4M with DSS. Faint dimers of His-CT2 can be detected *in situ* and the protein cross-linked by DSS into prominent dimers and tetramers. In contrast, His-CT2-4M protein exists only as monomers and there is no detectable cross-linking by DSS. (**D**) Expression of epitope-tagged PC2 and mutant PC2 on non-reducing SDS–PAGE. Wild-type PC2 migrates most prominently as dimeric species. Mutation of CC2 (PC2-4M) results in a predominant monomeric pattern with a faint dimeric species. PC2 mutants that include (R872X) or exclude (R742X) the CC2 region show a migration pattern similar to wild type or PC2-4M, respectively. (**E**) Co-immunoprecipitation of co-expressed HA-PC2 with Pk-PC2 or Pk-PC2-4M in HEK293 cells. Unlike CT2, mutation of CC2 in full-length PC2 (PC2-4M) does not abrogate full-length PC2 association. Pk is the epitope tag: GKPIPNPLLGLDST.

Of interest, the estimated frictional ratio (f/f_0) was 1.5 (His-CT2) and 2.19 (His-CT2-4M), respectively. Assuming that the major peak for each protein represents dimers and monomers, respectively, this suggests that dimerization results in a more compact structure than monomers.

CC2 is crucial for C-terminal oligomerization but not for oligomerization of full-length PC2

In solution, His-CT2 showed a tendency to form dimers visible on SDS–PAGE (Figure 2C). Brief cross-linking using the protein cross-linker disuccinimidyl suberate (DSS, 5 μM) showed that His-CT2 dimerized and oligomerized (Figure 2C). In contrast, His-CT2-4M showed no tendency to dimerize or oligomerize in the absence or the presence of DSS.

As reported earlier, full-length PC2 migrates as several species on non-reducing SDS–PAGE (Newby *et al*, 2002; Feng *et al*, 2008). Apart from a monomeric band (110 kDa), dimers (~220 kDa) were most prominent but higher order oligomers could also be visualized (Figure 2D). PC2-4M showed more prominent monomers and rather faint dimers. We generated two additional PC2 mutations: R742X, which excludes CC2 and R872X, which includes CC2. As shown in Figure 2D, the presence of CC2 (PC2-R872X) correlates closely to the wild-type PC2 migration pattern with prominent dimers. However, deletion of CC2 (PC2-R742X) results in more prominent monomers but does not abrogate formation of dimers. We next tested whether disruption of CC2 would abolish the ability of full-length PC2 to bind to wild-type PC2 in co-IP assays. As shown in Figure 2E, PC2-4M could still bind to wild-type PC2. Other mutations (PC2-M849P) gave similar results (data not shown).

CC2 mediates tail-to-tail dimerization of PC2 and induces ER cisternae stacks

To examine the subcellular expression of PC2, HEK 293T cells were processed for immunofluorescence using our N-terminally directed hPC2 antibody (N-PC2; Supplementary Figure 2A and B). HEK 293T cells expressing full-length untagged hPC2 exhibited two types of inclusions that stained brightly with the N-PC2 antibody. In most cells, PC2 localized in concentric patches (called whorls), which were dispersed around the nucleus throughout the cytosol (Figure 3A), and

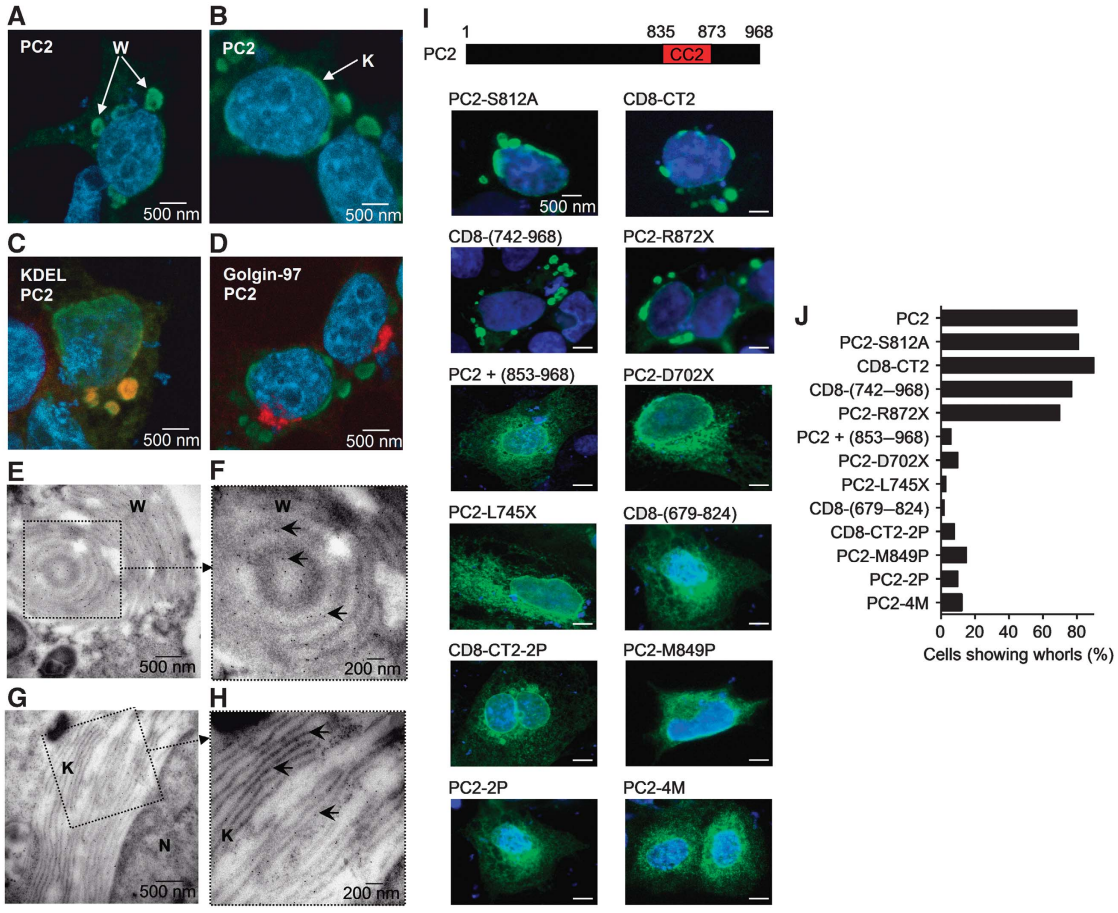

Figure 3 CC2-mediated dimerization of PC2 causes formation of stacked ER cisternae. (**A**, **B**) Representative distribution of full-length PC2 in transiently transfected HEK 293T cells. Cells were stained with the N-PC2 antibody (green) and imaged by confocal microscopy. W and K indicate the formation of whorls and karmellae. (**C**, **D**) PC2 (green) was co-stained with KDEL (**C**, red) or Golgin-97 (**D**, red) in HEK 293T cells. Cells were representative of >50 cells and imaged by confocal microscopy. KDEL, but not Golgin-97, co-localises with PC2 within whorls. Shown are overlays but individual channels can be seen in the Supplementary Figure 3B. (**E**–**H**) Immunogold electron microscopy showing the specific location of PC2 within whorls (W) and karmellae (K) in transfected HEK 293T cells. (**F**, **H**) High magnification images showing 1 nm colloidal gold particles (arrows) located in the layers of double-membrane ER. N, nucleus. (**I**) Representative pattern of expression of PC2 mutants. HEK 293T cells were transiently transfected with cDNAs as indicated and stained 48 h later with either N-PC2 or anti-CD8. Note that PC2 and CT2 with truncated or disrupted CC2 distribute uniformly in the ER. (**J**) The percentage of PC2-expressing cells showing whorls is plotted for the various PC2 constructs. Quantification was made from over 100 cells for each condition.

in elongated loops adjacent to the outer nuclear envelope, which we will refer below as karmellae (Figure 3B) (Wright *et al*, 1990). Accumulation of PC2 in karmellae and whorls was observed after transfection in a variety of cell types, including CHO, COS-7 and MDCK cells (Supplementary Figures 2C and 3A). Within whorls, PC2 co-distributed with typical ER-resident proteins including calnexin, protein-disulfide isomerase (PDI) and KDEL (Figure 3C), consistent with these structures being of ER origin. Neither the Golgi apparatus markers, Golgin-97, GM130 and βCOP nor the endosomal or lysosomal markers (EEA1, rab7, LAMP1), were detected in PC2-labelled structures (Figure 3D; Supplementary Figure 3B and data not shown). HEK 293T cells overexpressing mPKD2L1 (TRPP3), which displays an identical coiled-coil domain, also displayed brightly stained whorls (Supplementary Figure 2D). However, neither mPKD2L2 (TRPP5), hTRPC1, hTRPV4, mTRPM8, mTRPA1 nor mPC1 or PKD1L3 caused remodelling of reticular ER (Supplementary Figure 2E–K).

To further characterize the effect of PC2 expression on ER structures, we used transmission electron microscopy (EM). A commonly encountered ultrastructural feature in cells overexpressing PC2 was ordered arrays of concentric multilayered ER membranes arranged in a non-random manner (Supplementary Figure 4A–D). Adjacent cisternae were separated by a narrow cytoplasmic space that averaged ~10 nm (Supplementary Figure 4D). Immunoelectron microscopic localization of PC2 with N-PC2 or anti-HA antibodies in ultrathin cryosection of HEK cells showed that colloidal gold particles located specifically in the layers of double-membrane ER (Figure 3E–H; Supplementary Figure 4E–H).

To test the contribution of PC2 domains to the induction of perinuclear membrane layers, we constructed a series of PC2 mutants (Supplementary Figure 5). Cells expressing the channel-dead mutant PC2-D511V (Ma *et al*, 2005; Bai *et al*, 2008a), assembled karmellae and whorls, indicating that ER reorganization is not influenced by ion transport (data not shown). Likewise, mutation at position 812 (PC2-S812A, Figure 3I and J) or destruction of the acidic cluster (PC2-D815-17A, not shown) had no effects on the ability of PC2 to induce ER cisternal stacks. Deletion of the N-terminal region up to aa742 (CD8-742–968) also had no effects on ER remodelling, whereas expression of C-terminal truncation

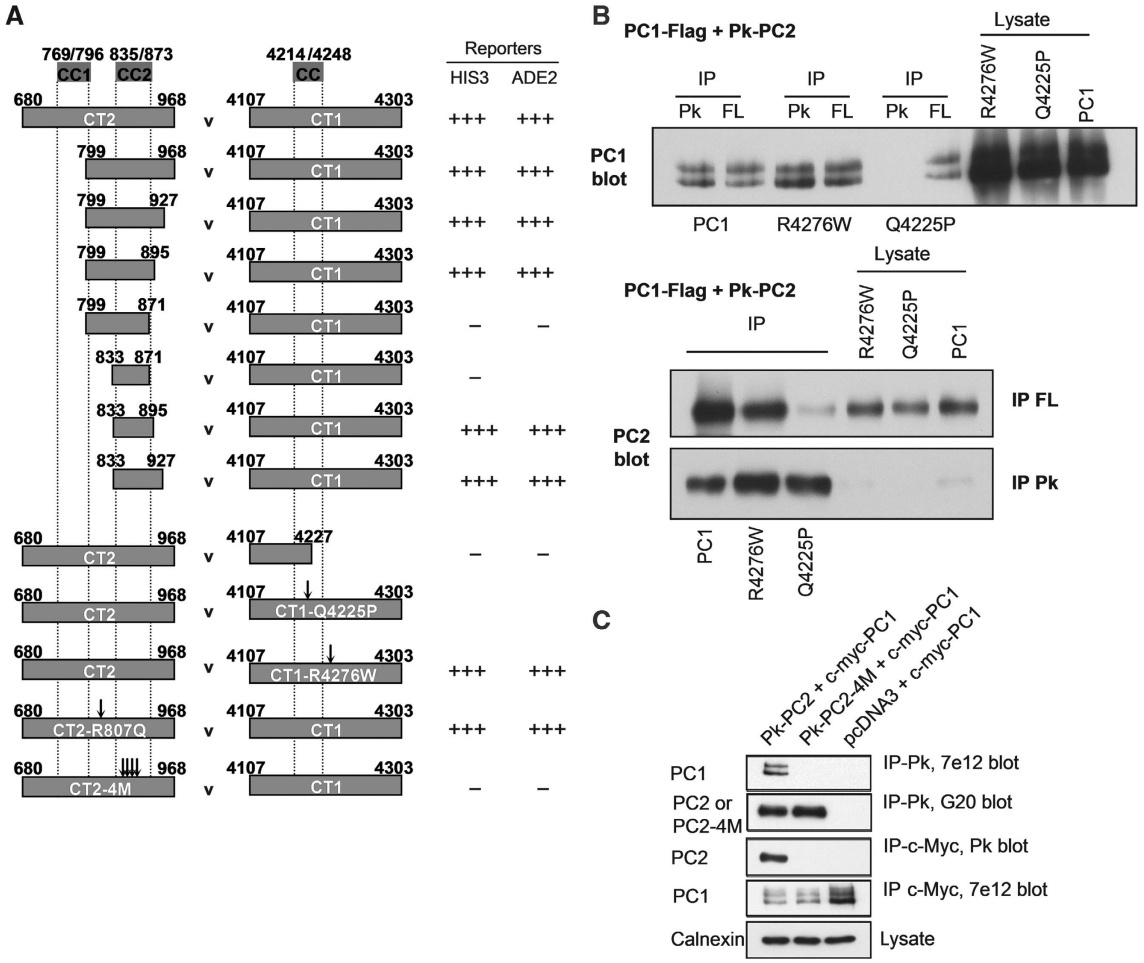

Figure 4 The integrity of CC2 is essential for the formation of a heteromeric PC1/PC2 complex. (**A**) Yeast two-hybrid assays with CT2 or deletion mutants as bait and full-length CT1 as prey. The minimal CT2 sequence essential for CT2/CT1 interaction was (833–895), which includes the CC2 domain (833–873). Mutations in CC2 (CT2-4M) abolished the CT2/CT1 association. Naturally occurring PC1 mutations, which either remove (R4227X) or disrupt (Q4225P) the coiled-coil domain in CT1 also abolished CT1/CT2 interactions but other polymorphisms (PC2-R807Q and PC1-R4276W) did not. Coiled-coil domains are indicated. (**B**, **C**) Co-immunoprecipitation of full-length PC1 and PC2 in HEK293 cells. (**B**) PC1 mutations in the coiled-coil domain (Q4225P) disrupt PC1/PC2 association. (**C**) CC2 mutations in full-length PC2 (PC2-4M) disrupt the formation of a PC1/PC2 complex. The 7e12 antibody recognizes PC1 and G20 antibody recognizes PC2.

mutants (PC2-D702X and PC2-L745X) failed to generate cisternal stacks (Figure 3I and J), indicating that the ER membrane proliferation-inducing signal resides in CT2. Deletion of CT2 distal to CC2 (PC2-R872X) had no effects on whorls formation, whereas deletion of CC2 (CD8-679–824) prevented the formation of stacked pairs of ER membranes (Figure 3I and J). Co-expression of a CC2-binding domain (853–968) lacking transmembrane spans, together with full-length PC2, prevented remodelling of reticular ER (Figure 3I). Furthermore, PC2-expressing cells with point mutations in CC2 no longer exhibited ER membrane reorganization. Collectively, these data suggest that homotypic interaction between CC2 domains of PC2 located on apposing ER membranes can differentiate reticular ER into stacked lamellae (Supplementary Figure 9).

CC2 does not bind PC1 but is required for heteromerization

Y2H assays were performed using CT2 or its truncations to delineate the minimal interacting regions for heterodimerization with the C-terminus of PC1 (CT1, 4107–4303aa, see Supplementary Figure 5). The minimal heterodimerization domain in CT2 required for CT1 binding was aa833–895 (Figure 4A). However, the shorter sequence 833–871, which corresponds to CC2, sufficient for CT2 self-association, was insufficient for CT2/CT1 binding. As expected, described human mutations that truncated (R4227X) or disrupted (Q4225P) the coiled-coil domain (L4214–R4248) of PC1 abolished CT1/CT2 interaction. In contrast, two other likely human polymorphisms, PC2-R807Q and PC1-R4276W, had no effect (Figure 4A). Most surprisingly, however, CC2 mutations (PC2-4M) in CT2 also abolished CT2/CT1 interaction, indicating that CC2 is necessary but not sufficient for CT2/CT1 binding.

To directly test the importance of CC2 for CT1 binding, we used an maltose-binding protein (MBP) fusion of CT1 and analysed its ability to pull-down Thio-CT2 or Thio-CT2-4M (Supplementary Figure 6A). MBP itself showed no binding to either protein but Thio-CT2-4M showed a marked reduction in binding to MBP-CT1 compared with Thio-CT2 (Supplementary Figure 6A). This confirmed the importance of the CC2 domain for direct binding to CT1.

PC1 C-terminus binding causes structural changes in CT2

2D NMR was then used to assess the intermolecular and intramolecular association of CT2. The 2D ^{1}H ^{15}N heteronuclear single quantum coherence spectrum of CT2 shows poor chemical shift dispersion and a mixture of sharp and broad signals with far fewer signals than would be expected for a 288-residue protein (Supplementary Figure 6B). Mutation of CC2 (CT2-4M) only gave a slightly sharper NMR spectrum implying that most of the conformational exchange occurs as a result of a weak intramolecular rather than an intermolecular-binding event. This possibility is supported by the observation that the broadening is not dependent on the concentration of CT2 protein (data not shown).

The addition of just over one equivalent of unlabelled CT1 produced large changes to the NMR spectrum of CT2 implying an interaction between the two proteins (Supplementary Figure 6B). Further, the addition of unlabelled CT1 produced a large increase in the number of signals and significantly reduced the differential broadening seen in CT2 alone. We conclude that the binding of CT1 to CT2 leads to a marked reduction of the intramolecular-binding event that led to the line broadening.

Addition of the CT1-R4227X mutant to CT2 had a much reduced effect on the CT2 spectrum. The only signal in the NMR spectra that can be assigned with certainty is the signal that comes from the side-chain of W916 of CT2. This signal is broadened in CT2-4M and is split into three on addition of CT1 presumably because of multiple bound conformations. These changes again confirm that the binding events involve the C-terminal end of CT2. Addition of unlabelled CT1 or CT1-R4227X to ^{15}N-labelled CT2-4M had very little effect (Supplementary Figure 6B).

Finally, we established that full-length PC1 and PC2 could interact using expression of epitope-tagged PC1-FLAG and Pk-PC2 in HEK 293T cells (Figure 4B). Deletion (R4227X, not shown) or disruption (Q4225P) of the coiled-coil domain of PC1 abolished PC1/PC2 interaction. However, disruption of CC2 (Pk-PC2-4M) also completely abolished interaction with PC1 (PC1-myc), indicating that CC2 is essential for PC1 binding (Figure 4C).

CC2 mutations prevent the formation of functional PC1/PC2 channel complexes in the PM

The effects of disrupting CC2 on the function of PC1/PC2 complexes were tested using whole-cell perforated patch-clamp recordings of sympathetic cells 48 h after intranuclear delivery of cDNAs (Delmas *et al*, 2004). Cells co-expressing full-length PC2 and PC1 displayed a standing inward current with a mean amplitude of -3.5 ± 0.45 pA/pF at -60 mV, which was inhibited by amiloride (100 μM), a typical but unspecific blocker of PC2 channels (Figure 5B) (Delmas *et al*, 2004; Bai *et al*, 2008a). This current had a reversal potential of -1 ± 2 mV ($n = 7$), typical of PC2. Combined visualization of PC2 and PC1 revealed multiple areas of co-localization of the two proteins at the cell surface (Supplementary Figure 7A). Amiloride-sensitive current was not detected in mock cells (expressing E-GFP, not shown) or cells expressing PC1 or PC2 alone (Figure 5A). To provide additional evidence that amiloride-sensitive current was carried by PC2, recordings were made in cells co-expressing PC1 and the channel-dead mutant PC2-D511V (Figure 5C). Mutations in PC1 (P4209X and R4227X) that truncated the coiled-coil domain in CT1 and abolished PC2 interaction occluded amiloride-sensitive currents (Figure 5D and J), although both PC1 mutants remained targeted to the PM (not shown, see Delmas *et al*, 2004). We next tested whether disruption of CC2 would abolish PC1/PC2 currents. None of the cells expressing the CC2 mutants together with full-length PC1 exhibited amiloride-sensitive currents (Figure 5E–G). In addition, the pathogenic mutation (PC2-R845X) produced no currents when co-expressed with PC1 (Figure 5H and J). S812A mutation within PC2 did not abolish amiloride-sensitive PC1/PC2 current (Figure 5I and J).

CC2 mutations prevent the formation of PC1/PC2 complexes at PM-ER junctions

The observation that ER-anchored PC2 can associate with some pools of surface PC1 in native tissues (Newby *et al*, 2002), suggests that the PC1/PC2 complex may function as a receptor-Ca^{2+}-release channel cross-linking the plasmalemma to the ER. To test this possibility, we measured intracellular Ca^{2+} mobilization in patch-clamped sympathetic cells in response to application of MR3, which functions as a PC1 activating antibody (Delmas *et al*, 2004; Bai *et al*, 2008a). In cells co-expressing PC1 and PC2, MR3 produced a large increase in cytosolic Ca^{2+} ($\Delta[Ca^{2+}]_i = 372 \pm 35$ nM) that declined slowly with a time constant of 2–8 min (Figure 6A and C). These Ca^{2+} responses were absent in cells expressing PC2 or PC1 alone (Figure 6A and C). Although the rise in Ca^{2+} was reduced on switching to a Ca^{2+}-free solution, MR3 still produced a significant rise in cytosolic Ca^{2+} when applied in a Ca^{2+}-free solution ($\Delta[Ca^{2+}]_i = 92 \pm 9$ nM) (Figure 6B and C), implying mobilization of Ca^{2+} from intracellular stores. Neither PC1/PC2-D511V-, PC1-P4209X/PC2- nor PC1/PC2-R824X-expressing cells responded to MR3 challenge (Figure 6B and C), indicating that integral PC1 and CC2-containing PC2 are required for MR3 mobilization of intracellular Ca^{2+}. In addition, prior depletion of ER Ca^{2+} stores using the ER Ca^{2+}-pump inhibitor thapsigargin (500 nM), fully prevented Ca^{2+} release in response to MR3 in PC1/PC2-expressing cells (Figure 6D).

Whether ER-anchored PC2 was required for MR3-induced Ca^{2+} mobilization was tested in cells pre-loaded with an anti-PC2 blocking antibody directed against the N-terminal cytosolic domain of PC2 (1:100, Delmas *et al*, 2004). This procedure prevented MR3-mediated Ca^{2+} mobilization ($\Delta[Ca^{2+}]_i = 7 \pm 5$ nM) in the absence of external Ca^{2+} (Figure 6F). We confirmed the specificity of the anti-PC2 blocking antibody in inside–out patch recordings of PC1/PC2 channel activity (Supplementary Figure 7B).

In addition, other treatments including 24 h pre-treatment with pertussis toxin (PTX), U73122, (10 μM), xestospongin C (2 μM) and the specific CK2 inhibitor 4,5,6,7-tetrabromo-2-azabenzimidazole (TBB, 10 μM) also had no effects on MR3 responses (Figure 6G). Moreover, intracellular dialysis of GDP-β-S (2 mM), heparin (1 mg/ml) and 8-NH_2-cADPR (50 μM) all failed to prevent MR3-induced Ca^{2+} mobilization (Figure 6E and G), indicating that Ca^{2+} release through ER-anchored PC2 was not contingent on the activation of PLC, $InsP_3$Rs or ryanodine receptors.

The effects of MR3 were also assessed on ER $[Ca^{2+}]$ (Supplementary Figure 7C). Ca^{2+} measurements in intracellular

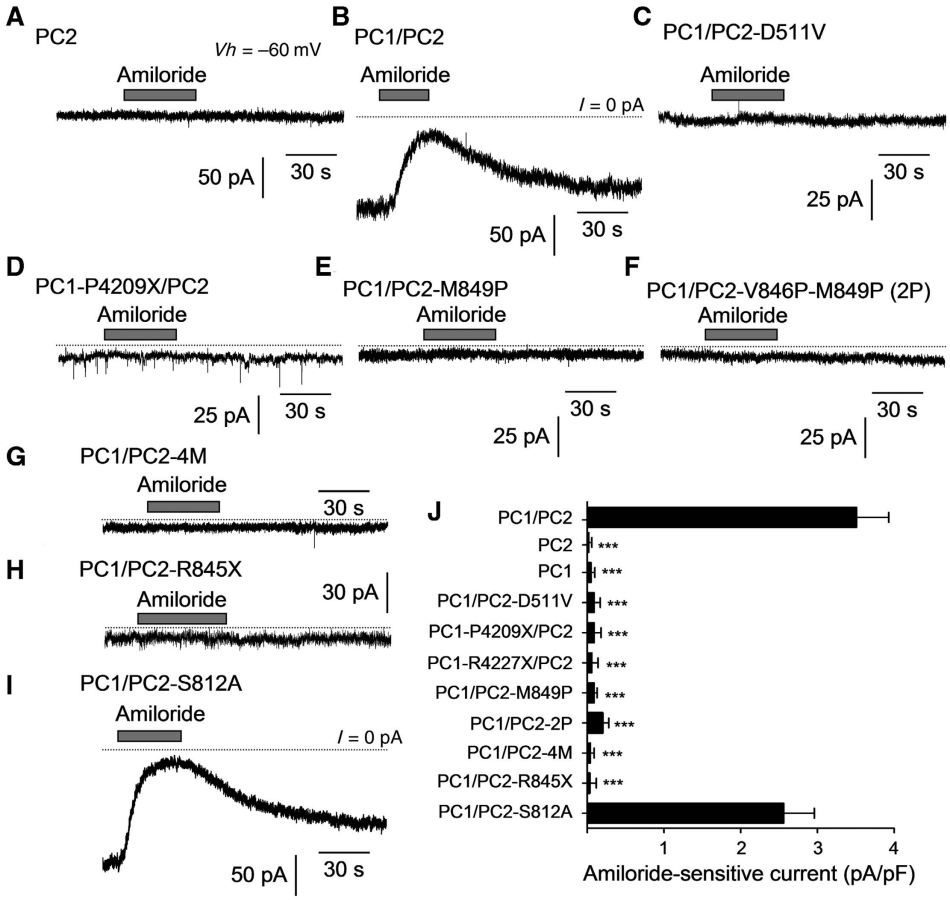

Figure 5 CC2 mutations disrupt plasmalemmal PC1/PC2 ion channel complex. (**A–I**) Standing inward currents recorded at a holding potential of −60 mV in sympathetic cells expressing PC2 (**A**), PC1/PC2 (**B**), PC1/PC2-D511V (**C**), PC1-P4209X/PC2 (**D**), PC1/PC2-M849P (**E**), PC1/PC2-V846P-M849P (**F**), PC1/PC2-4M (**G**), PC1/PC2-R845X (**H**) and PC1/PC2-S812A (**I**). PC2-mediated currents were detected from amiloride block (100 μM). Cells were voltage clamped using the perforated-patch method. Note that amiloride blocks a steady inward current in cells expressing PC1/PC2 but not in cells co-expressing PC1 and CC2 mutants. The dashed lines indicate the zero current baseline. (**J**) Amiloride-sensitive currents normalized to cell capacitance are shown for the different conditions. Bars represent mean ± s.e.m. for 4–12 cells. $***P<0.001$.

organelles were made using the Ca^{2+}-sensitive probe Mag-fura-2 AM. To eliminate cytosolic dye molecules and detect only the signal originating from intracellular compartments, cells were patched in the whole-cell mode to achieve intracellular wash out of cytosolic Mag-fura-2 (Supplementary Figure 7C). About 15 min after achieving the whole-cell recording mode in a cell co-expressing full-length PC1 and PC2, the cell response to MR3 application consisted of a transient decrease in Mag-fura-2 ratio, corresponding to an average decrease in ER $[Ca^{2+}]$ from 352 ± 60 to 195 ± 55 μM ($n=5$). When the anti-PC2 blocking antibody was subsequently added to the patch pipette, the expected decrease in ER $[Ca^{2+}]$ could not be seen, although Ca^{2+} stores could still be depleted by adding caffeine to the bath (Supplementary Figure 7C).

We next examined whether disruption of CC2 would prevent MR3-induced cytosolic Ca^{2+} mobilization in cultured HEK 293T cells loaded with the Ca^{2+}-binding dye Fura-PE3 AM and analysed with fluorometric ratio imaging. Cells co-expressing the CC2 mutants PC2-M849P, PC2-4M or PC2-2P with full-length PC1 and exposed to MR3 did not show Ca^{2+} rises when bathed with a Ca^{2+}-free external medium (Figure 6H–K). In contrast, MR3 caused transient rises in intracellular Ca^{2+} in cells co-expressing full-length PC1 and WT PC2 or PC2-S812A (Figure 6H, I and K). Collectively, these data show that CC2 is necessary for the formation of PC1/PC2 at PM-ER junctions.

CC2 mutants can form ER-anchored Ca^{2+}-release channels activated by PLC-coupled membrane receptors

Although CC2 mutants of PC2 can no longer form functional complexes with PC1, they maintain their ability to form oligomers (Figure 2). Therefore, we examined Ca^{2+} release from intracellular stores in response to ATP (400 μM) in cells expressing the CC2 mutants PC2-M849P and PC2-4M (Figure 7). ATP-mediated Ca^{2+} transients had significantly ($P<0.01$) higher amplitudes in cells expressing PC2-M849P (Δ ratio, 0.44 ± 0.06) and PC2-4M (Δ ratio, 0.39 ± 0.03) compared with mock-transfected cells (Δ ratio, 0.21 ± 0.03), suggesting that PC2 with disrupted CC2 can form functional Ca^{2+}-release channels. ATP responses had identical amplitude in the absence of external Ca^{2+}, showing that the release of Ca^{2+} derives from intracellular stores (Supplementary Figure 8). In addition, PC2 activation by ATP appeared downstream to $InsP_3$ receptors because it was prevented by 2-APB (100 μM) (Supplementary Figure 8).

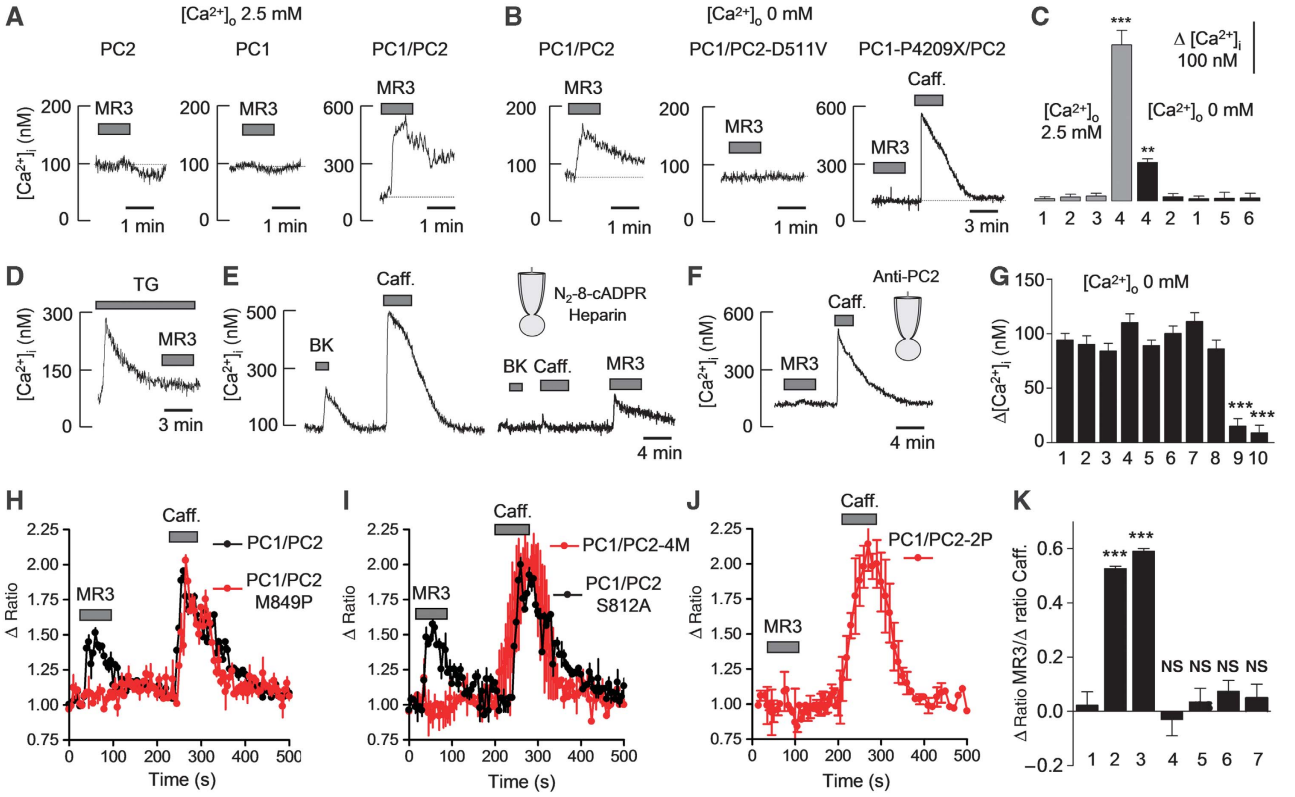

Figure 6 CC2 mutations disrupt PC1/PC2 complex (PlasmaERosome) at PM-ER junctions. (**A**) $[Ca^{2+}]_o = 2.5$ mM. Representative Ca^{2+} responses to MR3 (1:100) applied for 1 min in sympathetic cells expressing PC2, PC1 and PC1/PC2. Note that MR3 increases intracellular Ca^{2+} only in the cell co-expressing PC1 and PC2. (**B**) Nominally Ca^{2+}-free external solution (0 mM external Ca^{2+} plus 1 mM EGTA). Ca^{2+} responses to MR3 in cells expressing PC1/PC2, PC1/PC2-D511V and PC1-P4209X/PC2. MR3-induced Ca^{2+} increase still occurs in PC1/PC2 cells but not in PC1/PC2-D511V and PC1-P4209X/PC2-expressing cells. Note that the integrity of the intracellular Ca^{2+} stores was routinely tested with caffeine (Caff., 10 mM). (**C**) MR3-induced rise in $[Ca^{2+}]_i$ in cells expressing PC1 (1), PC2 (2), PC2-D511V (3), PC1/PC2 (4), PC1-P4209X/PC2 (5) and PC1/PC2-R824X (6) in the presence (grey bars) or absence (black bars) of external calcium. Bars represent mean ± s.e.m. for 5–9 cells. $^{**}P<0.01$; $^{***}P<0.001$, compared with PC1/PC2-D511V-expressing cells. (**D**) $[Ca^{2+}]_o = 0$ mM. MR3-induced Ca^{2+} mobilization was blocked in PC1/PC2-expressing cells by depleting intracellular Ca^{2+}-stores with thapsigargin (TG, 500 nM). (**E**) $[Ca^{2+}]_o = 0$ mM. MR3-induced Ca^{2+} mobilization is not suppressed in PC1/PC2-expressing cells in which IP3Rs and ryanodine receptors are blocked by heparin (1 mg/ml) and N_2-8-cADPR (50 μM), respectively. Ca^{2+} rises in response to bradykinin (BK, 500 nM) and caffeine (10 mM) were used as internal controls. (**F**) $[Ca^{2+}]_o = 0$ mM. MR3-induced Ca^{2+} mobilization is abolished in PC1/PC2-expressing cells loaded with an anti-PC2 blocking antibody (1:100). (**G**) MR3-induced rise in $[Ca^{2+}]_i$ in cells expressing PC1/PC2 in control conditions (1) and following exposure to U73122 (10 μM) (2), PTX (1 ng/ml for 24 h) (3), anti-$G\alpha_{q/11}$ antibody (intracellular dialysis for 15 min, 1:100) (4), xestospongin C (20 μM) (5), GDP-β-S (2 mM, intracellular dialysis) (6), TBB (10 μM for 1 h) (7), heparin/N_2-8-cADPR cocktail (intracellular dialysis for 10 min) (8), thapsigargin (500 nM) (9) and anti-PC2 antibody (intracellular dialysis, 1/100) (10). Bars represent mean ± s.e.m. of 6–11 cells. $^{***}P<0.001$, compared with control conditions (1). All data collected with $[Ca^{2+}]_o = 0$ mM. (**H–K**) $[Ca^{2+}]_o = 0$ mM. Averaged calcium transients in response to MR3 (1:100) and caffeine (10 mM) exposures in HEK 293T cells expressing PC1/PC2 or PC1/PC2-M849P (**H**), PC1/PC2-4M and PC1/PC2-S812A (**I**) and PC1/PC2-V846P-M849P (2P) (**J**). Data points represent mean ± s.e.m. of 30–65 cells. (**K**) Bar graph summarizing MR3-induced $[Ca^{2+}]_i$ rise normalized to caffeine-induced $[Ca^{2+}]_i$ rise in cells expressing PC2 (1), PC1/PC2 (2), PC1/PC2-S812A (3), PC1/PC2-M849P (4), PC1/PC2-4M (5), PC1/PC2-2P (6) and PC1/PC2-D511V (7). Bars represent mean ± s.e.m. of 30–65 cells. $^{***}P<0.001$; NS, non-significant, compared with cells expressing PC1/PC2-D511V.

To assess whether CC2 mutant channels were as 'functional' as wtPC2 channels, we co-expressed wtPC2 with PC2-4M or PC2-M849P to favour the formation of heteromeric channels (Figure 7D–F). ATP responses in these cells were undistinguishable from ATP responses in cells expressing CC2 mutants alone. However, cells transfected with low concentrations of wtPC2 cDNA (0.5 μg)—to prevent ER rearrangement and whorl formation—showed significantly enhanced ATP responses compared with cells expressing PC2 channels with CC2 mutations (Figure 7F). These data indicate that CC2 mutations abrogated PC1/PC2 functions but not PC1-independent functions of PC2. In addition, channels containing PC2 subunits with CC2 mutations have reduced activity compared with wild-type channels.

Expression of CC2 mutants in zebrafish causes pronephric kidney cyst formation and little features of situs inversus

Zebrafish pkd2 ATG morpholino (*pkd2ATGMO*) blockade of endogenous PC2 protein translation cause cyst formation in the glomerulus and pronephric tubules in conjunction with changes in body axis curvature, hydrocephalus and organ situs (Sun *et al*, 2004; Obara *et al*, 2006; Sullivan-Brown *et al*, 2008; Wessely and Obara, 2008). All these features can be rescued by co-injection of *hPKD2* capRNA, indicating that the functions of human and zebrafish PC2 are interchangeable (Obara *et al*, 2006; Streets *et al*, 2006; Feng *et al*, 2008). Injection of both *PKD2-M849P* and *PKD2-4M* capRNAs in zebrafish induced hydrocephalus, body axis curvature, heart

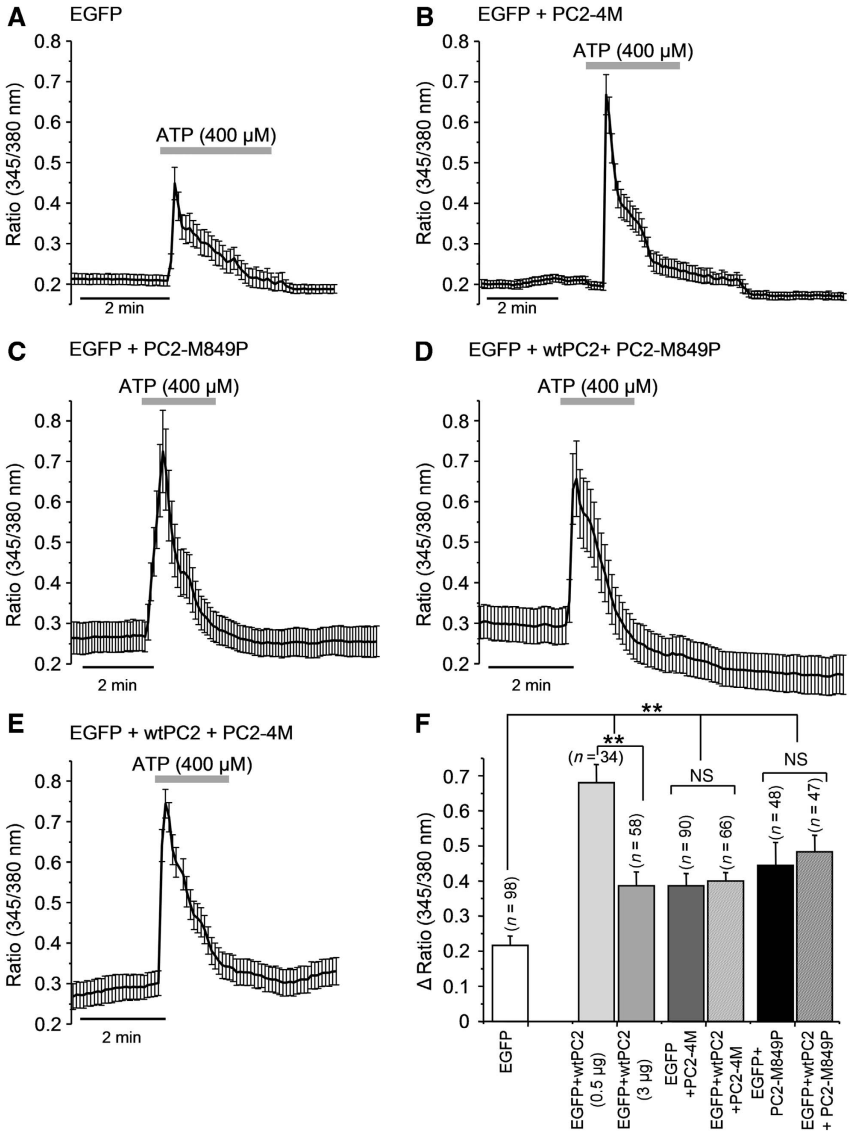

Figure 7 PC2 channels with CC2 mutations can form receptor-operated Ca^{2+}-release channels. Averaged calcium transients in response to ATP application (400 μM) in HEK 293T cells expressing EGFP ($n = 11$) (**A**), EGFP + PC2-4M ($n = 11$) (**B**), EGFP + PC2-M849P ($n = 21$) (**C**), EGFP + WT PC2/PC2-M849P ($n = 10$) (**D**) and EGFP + WT PC2/PC2-4M ($n = 17$) (**E**). Grey horizontal bars indicate duration of ATP application. (**F**) Histogram showing averaged rise in $[Ca^{2+}]_i$ induced by ATP in cells expressing EGFP (3 μg cDNA), EGFP + WT PC2 (0.5 μg cDNA, no whorls), EGFP + WT PC2 (3 μg cDNA, whorl formation), EGFP + PC2-4M (3 μg cDNA), EGFP + WT PC2/PC2-4M (1.5 μg cDNA each), EGFP + PC2-M849P (3 μg cDNA) and EGFP + WT PC2/PC2-M849P (1.5 μg cDNA each). Bars represent mean ± s.e.m. of 34–98 cells. $^{**}P < 0.01$; NS, not significant.

edema and cystic pronephro similar to the *pkd2* morphants (Figure 8D and E). The pronephric cysts were validated by histological cross-sections. Human *PKD2*, *PKD2-M849P* and *PKD2-4M* capRNAs expression in the zebrafish larvae was confirmed by nested RT–PCR using *hPKD2*-specific primers and further sequencing (Figure 8F). Out of >200 embryos injected for each condition, cyst formation in the pronephros was observed in 2, 88, 80 and 94 % of embryos injected with *hPKD2*, *hPKD2-M849P*, *hPKD2-4M* and *pkd2ATGMO*, respectively (Figure 8G).

Current models for the initiation of a left–right asymmetry (LR) breaking event include the function of PC2 but not PC1 (McGrath *et al*, 2003). It had been previously shown that disruption of zebrafish *pkd2* affects heart loop asymmetry (Bisgrove *et al*, 2005; Obara *et al*, 2006; Schottenfeld *et al*, 2007). In normal embryos, the ventricle of the heart loops to the right, whereas the atrium loops to the left. However, *pkd2ATG* morphants showed randomized heart looping with roughly 30% normal, 50% inverted and 20% midline (Figure 8H). Human CC2 mutant capRNAs expressed in zebrafish had weaker effects than *pkd2ATG* morphants on LR asymmetry, as heart looping was 65% normal, 25% inverted and 10% midline with *PKD2-M849P* capRNA and 72% normal, 21% inverted and 7% midline with *PKD2-4M* capRNAs (Figure 8H). LR organogenesis in embryos injected with control morpholino (universal control MO) was 96% normal, 2% inverted and 2% midline, results indistinguishable from embryos injected with *hPKD2* capRNA (94% normal, 4% inverted, 2% midline) (Figure 8H).

Discussion

Earlier work has indicated that PC2 can heterodimerize with PC1 through a C-terminal cytoplasmic interaction to form a

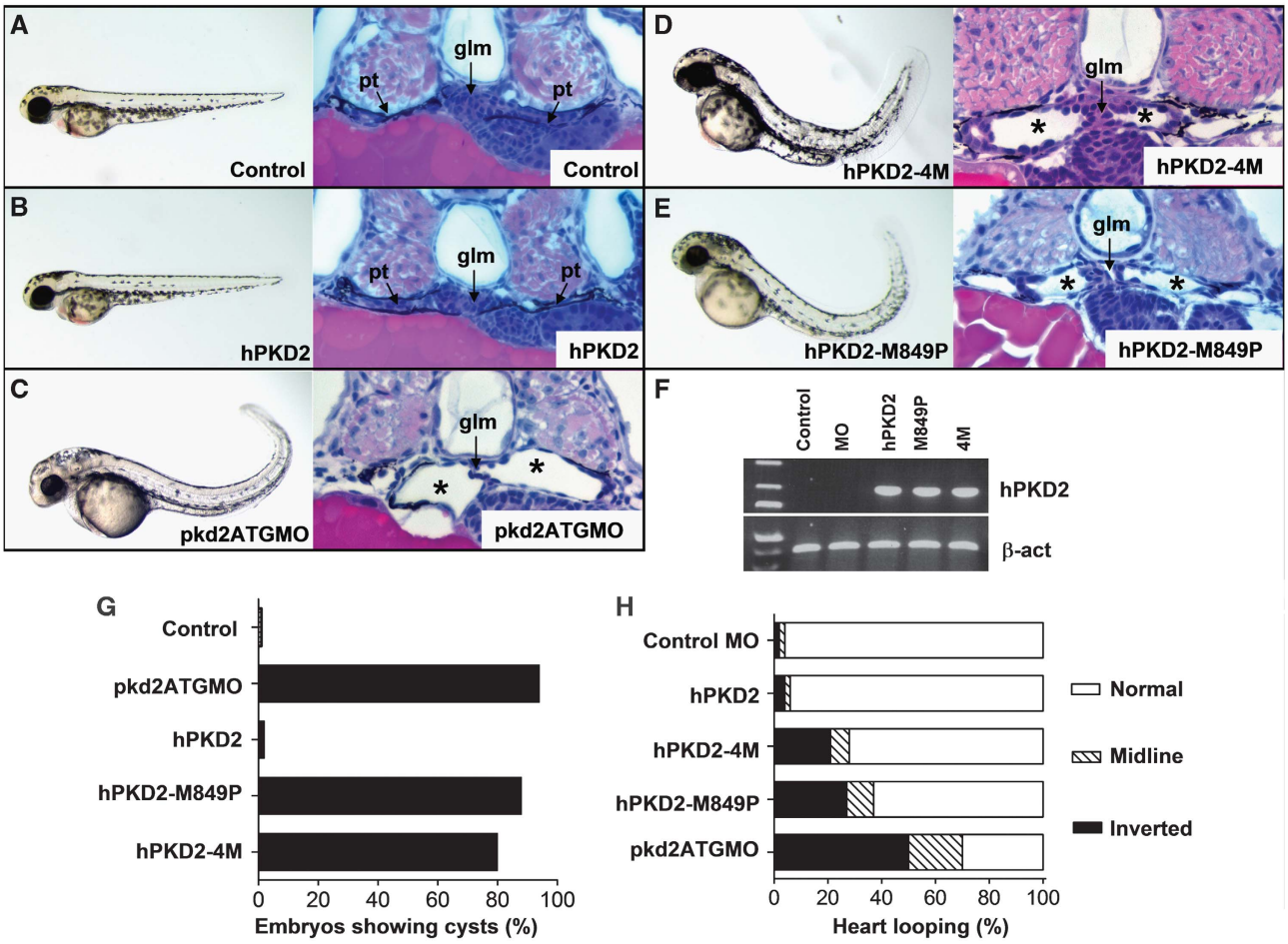

Figure 8 Human PKD2-M849P and PKD2-4M mRNA injected embryos exhibit pronephric cyst formation in zebrafish. (**A–E**) Whole-mount lateral view and cross-section of the glomerular (glm) and pronephric tubules (pt) on 48 hpf zebrafish larvae. *pkd2ATGMO*-injected embryos (**C**) and human *PKD2-4M* (**D**) and *PKD2-M849P* (**E**) capRNAs-injected embryos show pronephric cysts, hydrocephalus and body axis curvature. In the histological cross-sections, glomerular and pronephric tubule cysts (stars) are present. Control MO (**A**) and *hPKD2* capRNA (**B**) injected embryos show normal structure. (**F**) Injected *hPKD2* capRNA (upper panel) and β-actin (lower panel) are detected by RT–PCR. Control MO (control), *pkd2ATGMO* (MO), *hPKD2* capRNA (hPKD2), *hPKD2-M849P* capRNA (M849P) and *hPKD2-4M* capRNA (4M). (**G**) Histogram showing the percentage of embryos with pronephric kidney cyst formation. (**H**) Histogram showing the percentage of embryos with normal, midline or inverted heart looping. More than 200 embryos were injected for each condition. Difference between *hPKD2* mutants and either *hPKD2 or pkd2ATGMO* are significant ($P<0.05$).

multimeric receptor-ion channel complex. In addition, PC2 also exists as homomers (Newby *et al*, 2002; Feng *et al*, 2008) and can assemble into heteromultimeric complexes with other TRP channel subunits, serving different functions in different subcellular compartments (Köttgen *et al*, 2008; Bai *et al*, 2008a). Here, we have identified and functionally characterized a coiled-coil domain that is critical for CT2 dimerization and binding to PC1 but not for assembly of homomeric PC2 channels. This C-terminal dimerization domain of PC2 therefore acts as a molecular signature for PC1 recognition and thus specifies the formation of multimeric PC1/PC2 complexes.

Using a coiled-coil prediction algorithm, we identified a stretch of residues extending from S835 to A873 (CC2) that exhibits a strong probability for coiled-coil formation. This domain, which has also been reported recently by others (Celic *et al*, 2008; Yu *et al*, 2009), is distal to the previously identified coiled-coil domain (E772–L796) named here CC1 (Tsiokas *et al*, 1997). Coiled-coil domains critical for channel assembly have been identified in the C-terminal cytoplasmic tails of a number of ion channels, including Kv7 channels (Schmitt *et al*, 2000; Schwake *et al*, 2003), ether-à-go-go K^+ channels (Ludwig *et al*, 1997; Jenke *et al*, 2003) and TRP channels (Tsuruda *et al*, 2006; Phelps and Gaudet, 2007; Fujiwara and Minor, 2008). Although it is clear that CC2 is an assembly domain, it does not seem to have a prominent function in the self-association of full-length PC2 but rather fosters formation of heteromeric PC1/PC2 complex. We found that PC2 channels with CC2 deletions tetramerize, localize properly in the ER and are not inactive, indicating that CC2 is not critical for tetramerization, localization or proper function of the channel. This is in general agreement with earlier observations showing that naturally occurring PC2 mutants lacking the C-terminus (L703X, R742X) still form oligomers and co-immunoprecipitate full-length PC2, implying the presence of a proximal dimerization domain in the N-terminus of PC2 (Feng *et al*, 2008). At variance, a recent study suggested that CC2 forms a homotrimer (Yu *et al*, 2009). The threefold symmetry shown in Yu *et al* (2009) is difficult to reconciliate with the fourfold symmetry of

functional TRP channels (Tsuruda *et al*, 2006; Phelps and Gaudet, 2007) and with the recently described homo- and hetero-oligomeric PC2 channels (e.g. PC2/TRPV4 and PC2/TRPC1) (Bai *et al*, 2008a; Köttgen *et al*, 2008; Kobori *et al*, 2009; Zhang *et al*, 2009). It is therefore likely that the CC2 motif-containing helix oligomerizes differently as an isolated peptide than when embedded in the folded protein. It is well known that the oligomerization state and orientation of coiled-coil helices are highly sensitive to minor alterations in the sequence or the chemical environment. For example, the GCN4 leucine zipper, one of the most widely used model systems in coiled-coil research, has been converted from a parallel dimer to at least seven different topologies by (often just one) point mutation. Truncation is also known to affect the oligomerization state of coiled-coil domains. For example, in the S2 fusion subunit of SARS coronavirus, the full-length central coiled coil is a parallel trimer, whereas a truncated fragment is an anti-parallel tetramer (Deng *et al*, 2006). A construct from the SK_{Ca} channel, which encompasses much of the coiled coil, has been solved as a parallel trimer (Kim *et al*, 2008), even though the native receptor is known to be tetrameric. This effect has also been observed in ion channels homologous to PC2. It has recently been shown that the coiled coil of the KCNQ1 (Kv7.1) channel, which has been determined as a parallel tetramer (Wiener *et al*, 2008), switches to a parallel trimer on truncation of 10 residues from the C-terminal tetramer (Xu and Minor, 2009). These results emphasize the fact that small changes in the amino sequence can have drastic effects on the oligomerization state, switching a four-stranded coiled coil into a three-stranded coiled coil. It is noteworthy in this respect that the crystal structure of PC2 G833–G895 by Yu *et al* (2009) lacks 23 residues (896–919) from the putative parallel tetramer.

Deletional and site-specific mutagenesis assays clearly indicate that CC2, although not physically binding to the coiled-coil domain of PC1, is required for heterotypic interaction between PC1 and PC2. The domain responsible for heterodimerization with PC1 is just distal to CC2 and extends from aa872 to aa895, in agreement with earlier studies (Tsiokas *et al*, 1997; Yu *et al*, 2009). Interestingly, CC2 is conserved down to lower vertebrates and invertebrates, suggesting that it represents an evolutionarily critical functional domain. Although absent from most TRP channels, it is also conserved in PKD2L1, which binds to PKD1L3 to form a sour taste receptor (Ishimaru *et al*, 2006; LopezJimenez *et al*, 2006). This suggests that CC2 is likely to direct channel assembly in other cases and may represent a general strategy for the assembly of prototypical PC1/PC2-like complexes.

On the basis of our results and recent published data on PC2, general functions for the N- and C-terminal cytosolic domains can now be defined. The region N-terminal to the first TM is clearly required for proper PM subdomain localization of PC2 (Geng *et al*, 2006; Streets *et al*, 2006) and contains a dimerization site, which possibly in conjunction with transmembrane domains, regulates channel tetramerization (Feng *et al*, 2008). The C-terminus of PC2, although not essential for channel tetramerization, provides an essential scaffolding platform for heteromeric assembly with other proteins and molecules required for the regulation of channel activity (Ca^{2+}, PC1, TRPC1, $InsP_3R$) (Tsiokas *et al*, 1999; Koulen *et al*, 2002; Li *et al*, 2005; Celic *et al*, 2008). Our data therefore show that the function of CC2 goes well beyond just assisting channel assembly and constitutes a dedicated domain for the formation of supramolecular entities and the specification of different heteromeric PC2 complexes.

On overexpression, PC2 induces stable layer formation by mediating zippering interactions between opposing ER membranes (Supplementary Figure 9). CC2 was the signal responsible for ER cisternal stack formation because ER stacks were not present in untransfected cells and in cells transfected with constructs encoding CC2 mutants. Regular arrays of ER membranes, reminiscent of the cisternal stacks observed by us, have been previously noted in cells overexpressing ER-resident proteins including HMG-CoA reductase and $InsP_3Rs$ (Anderson *et al*, 1983; Takei *et al*, 1994). Here again, a crucial requirement for the formation of cisternal stacks was the property of the cytosolic domains of the overexpressed proteins to bind through homo/heterotypic interactions with proteins on adjacent ER membranes. As this phenomenon is not normally seen in epithelial kidney cells, the significance of exogenous PC2-induced cisternal stacks remains unclear. It may reflect, however, a potential mechanism of communication by polycystin proteins.

Assembly of PC1 and PC2 has been shown to reconstitute a large conductance, non-selective cation channel in the PM of host cells (Hanaoka *et al*, 2000; Gonzalez-Perrett *et al*, 2001; Delmas *et al*, 2004; Bai *et al*, 2008a). Consistent with reported data that PC1 is required to bring PC2 to the PM and co-assemble a polycystin complex, disruption of CC2 abolished ion channel activity of a PM PC1/PC2 complex. Besides functioning as an integral PM receptor/cation channel, our data also reveal for the first time that PC1/PC2 complex can function as a receptor/Ca^{2+}-release channel that regulates the activity of PC2 located in the ER but tethered close to the cell surface through its C-terminal interaction with PC1 (Koulen *et al*, 2002). These functional data accord well with earlier biochemical data showing that Endo H-resistant PC1 can interact with a pool of Endo H-sensitive PC2 in lateral cell membranes of renal epithelial cells (Newby *et al*, 2002). The complex between the two polycystins should be co-assembled in subdomains where plasma and ER membranes may be in close apposition, possibly through a mechanism akin to that described above for the formation of stacked ER membranes. A simplified view of the proposed organization of polycystin complexes is depicted in the Supplementary Figure 10. Physical linkage between proteins in the surface membrane and the ER are crucial for spatio-temporal coding of Ca^{2+} events (Delmas and Brown, 2002) and have been implicated in mediating CRAC channel activation (Luik *et al*, 2008), cross-talk between $InsP_3Rs$ and TRP channels (Birnbaumer *et al*, 2000; Delmas *et al*, 2002b) and excitation-contraction coupling in skeletal muscle.

To explore further the *in vivo* function of CC2, we analysed the effects by expressing hCC2 mutants in the zebrafish embryos. Examination of these embryos using both whole-mount phenotyping and histological section analysis provided strong evidence that CC2 is required for proper assembly and function of the polycystin complex in zebrafish. Expression of hCC2 mutant capRNAs was sufficient to induce pronephric cyst formation, body axis curvature and hydrocephalus. Further analysis indicated that expression of hCC2 mutants was as efficient as *pkd2ATG* morphants in causing pronephric cysts. This could be explained if human CC2 mutants form oligomeric channels with zebrafish PC2,

sequestering this subunit away from interacting with zebrafish PC1.

Similar to the *PKD2* KO mouse, zebrafish *pkd2* morphants exhibit a variety of organ laterality defects, supporting a conserved requirement for *pkd2* function in the left–right patterning (Pennekamp *et al*, 2002; Bisgrove *et al*, 2005; Obara *et al*, 2006). In contrast to the similar effects of CC2 mutant capRNA expression on pronephric cyst formation, they had lesser effects on cardiac left–right asymmetry compared with *pkd2* morphants. These data are consistent with the preserved but reduced ER Ca^{2+}-release channel activity of the CC2 mutants. As PC2 is normally ER localized in the absence of PC1, we hypothesize that ER-anchored PC2 (at the embryonic node) has a critical function in the development of left–right asymmetry.

In conclusion, the new dimerization domain we describe has helped clarify the previously proposed functions of PC2, both as a heteromeric complex with PC1 and as homomers. Mutations that disrupt the function of this domain or the coiled-coil domain in PC1 are likely to be pathogenic in cyst formation.

Materials and methods

In silico model of CC2

The coiled-coil region (CC2) of hPC2 was modelled using BeammotifCC. Further details are described in the Supplementary data section.

Yeast two-hybrid screening

Yeast two-hybrid assays were performed in the yeast strain AH109 containing ADE2, HIS3 and LacZ reporter genes under the control of the GAL4 upstream activating sequences as described earlier (Feng *et al*, 2008). Bait and prey constructs were co-transformed into yeast cells and positive co-transformants (containing both bait and prey plasmids) picked from selective medium SD/-LT (lacking tryptophan and leucine). These were restreaked onto selective media SD/-LTH (lacking tryptophan, leucine and histidine), SD/-LTH with 2 mM 3-amino-1, 2, 4-triazole (3-AT) and SD/-LTAH (lacking tryptophan, leucine, histidine and adenine), respectively, to activate the reporter genes HIS3 and ADE2. PC2 C-terminus (CT2, 680–968) and PC1 C-terminus (CT1, 4107–4303) or their truncations were subcloned into the bait (BD) vector pGBKT7 or prey (AD) vector pGADT7 (Clontech). Site-specific mutations of CT2 or CT1 were generated as described earlier (Streets *et al*, 2006). The constructs pGBKT7-53 (p53) and pGBADT7-T (SV40 T-antigen) were used as a pair of positive controls. Truncations of CT2 and CT1 that mimic two naturally occurring mutants lacking their respective interaction domains, that is PC2-R742X and PC1-R4227X, respectively, were generated as a pair of negative controls: pGADT7-CT2 (680–742) and pGBKT7-CT1 (4107–4227). At least three individual colonies were chosen from each plate to quantify growth.

DNA constructs and site-directed mutagenesis

Full-length hPKD1 and hPKD2 cDNAs were constructed as largely described (Delmas *et al*, 2004; Bai *et al*, 2008a; Streets *et al*, 2009; Ong *et al*, 1999a, b). Further details are described in the Supplementary data section.

Patch-clamp recording and intranuclear cDNA delivery

Cell lines and sympathetic neurons were cultured and transfected as described in the Supplementary data section (Delmas *et al*, 2002b, 2004). Currents were recorded using the variants of the patch-clamp technique. For both perforated-patch and patch-ruptured whole-cell recordings, the external solution consisted of (mM): NaCl, 110; $NaHCO_3$, 23; KCl, 3; $MgCl_2$, 1.2; $CaCl_2$, 2.5; HEPES, 5; D-glucose, 11; tetrodotoxin (TTX), 0.0005 (bubbled with a 95 % O_2-5% CO_2 mixture, pH 7.4). For perforated patch recording, the intracellular solution consisted of amphotericin-B (0.1 mg/ml in DMSO); K^+ acetate, 90 mM; KCl, 30 mM; $MgCl_2$, 3 mM and HEPES, 40 mM (adjusted to pH 7.3 with KOH, 290 mOsmol/l). For patch ruptured, the intracellular solution consisted of (mM): 109 KCl, 14 CsCl, 10 HEPES, 11 EGTA, 1 $MgCl_2$, 1 $CaCl_2$, 0.1 phosphocreatine, 2 MgATP and 0.2 Na_3GTP (pH 7.3). Pipettes had resistance of 3 MΩ. The MR3 antibody is a third generation polyclonal antibody made on the PC1 epitope described earlier (Delmas *et al*, 2004). Currents were measured with an Axopatch 200A amplifier (Axon Instruments), filtered at 2 kHz and analysed off-line with pCLAMP9. Cell membrane capacitance and series resistance compensations were applied. All experiments were performed at room temperature (RT) and drugs were applied by using a gravity-fed perfusion system.

Measurement of cytosolic $[Ca^{2+}]$

SCG cells: free $[Ca^{2+}]_i$ was estimated from indo-1 fluorescence using the ratiometric method. Briefly, cells were incubated with 5 μM indo-1-AM for 30 min and then superfused with standard bath solution for 15 min to allow ester hydrolysis. Dye-loaded cells were excited at 360 nm, and the 408/480 emission ratio was used to calculate intracellular free Ca^{2+}. Sample rate was 50 Hz. Calibration was achieved by whole-cell dialysis of SCG cells with intracellular solutions containing known concentrations of free Ca^{2+}. $[Ca^{2+}]_o$ was either 0 or 2.5 mM, as indicated. HEK 293T cells: coverslips with HEK 293T cells were loaded with fura-PE3 AM (2 μM) for 30 min (37°C, 5% CO2) in culture medium. Glass coverslips were then individually inserted in a specific chamber (Harvard Apparatus) and placed on the stage of an inverted epifluorescence microscope (Olympus IX71) equipped with a ×40, UApo/340-1.15 W water-immersion objective. Fura-PE3 was alternately excited at 345 and 380 nm, and ratios of the resulting images (345/380) were produced every 5 s. The source of excitation light was a xenon arc lamp, and excitation wavelength was selected by a fast excitation filter wheel (Illumination Systems MT20, Olympus). Digital images were sampled at 12-bit resolution by a fast-scan, cooled charge-coupled device (B/W CCD) digital camera (Orca-ER, Hamamatsu). All the images were background subtracted and controlled by Cell-R software (Olympus). Control experiments performed with EGFP-expressing cells not loaded with Fura-PE3 showed that at the wavelengths selected for Fura-PE3 fluorescence measurements, neither a fluorescence signal nor changes in intensity were detected. This indicates that in our experimental setup, there was no contribution of EGFP fluorescence to the Fura-PE3 signal.

Immunocytochemistry

Cell lines and primary neuronal cultures were fixed using 4% paraformaldehyde in phosphate-buffered saline (PBS) for 20 min followed by permeabilization (45 and 5 min, respectively) with 5% bovine serum albumin (BSA) and 0.1% Triton X-100 in PBS. Primary antibodies were incubated in blocking buffer (PBS, 5% BSA) for 1 h at RT. Secondary antibodies were incubated in blocking buffer for 1 h. Cells were incubated in DAPI (1:1000; Sigma) for 20 s and mounted in Mowiol (Calbiochem). A new anti-PC2 polyclonal antibody (NPC2) was generated: it was raised in rabbits against an N-terminal peptide of PC2 (CSRQAWSRDNPGFEAE, aa 82 to 97 in hPC2) common to rat, mouse and human sequences. Primary antibodies used and dilutions were: rabbit NPC2 (1:200), mouse monoclonal anti-FLAG (1:400; Sigma), rabbit anti-CD8-α (1:200; Santa Cruz Biotechnology), mouse monoclonal anti-HA (1:400; Sigma), mouse monoclonal anti-Golgin-97 (1:200; Molecular probes) and mouse monoclonal anti-KDEL (1:200; Stressgen Bioreagents). Antibodies against calnexin, PDI, GM130, βCOP, EEA1, Rab7 and LAMP2 were from Abcam or BD Biosciences (1/300–1/800). Goat anti-rabbit IgG Alexa Fluor546 (1:200; Molecular Probes), goat anti-mouse IgG Alexa Fluor488 (1:200; Molecular Probes), goat anti-rabbit FITC (1:200; Jackson ImmunoResearch) and goat anti-mouse TRITC (1:200; Jackson ImmunoResearch) were used as secondary antibodies. Images were acquired using an inverted epifluorescence microscope (Olympus IX 71) equipped with a ×60 UPLFLN oil-immersion objective and configured for multifluorescence image capture. Images were acquired and analysed using Cell-R Imaging software (Olympus).

Immunoblotting and immunoprecipitation assays

Cell lysates were obtained by extraction at 4°C using the lysis buffer (mM): Tris (pH 7.5), 20; NaCl, 200; EDTA, 1 and 1% Triton X-100 and 0.5% BSA in the presence of a complete protease inhibitor cocktail (Roche Applied Science), rocking for 20 min and centrifugation for 10 min at 10 000 g. Protein concentration was estimated

using the BCA protein assay kit (Pierce). Protein extracts were separated on 7.5% or 10% SDS–polyacrylamide gels and transferred to 0.45 μm nitrocellulose membranes. Membranes were blocked with 5% skim milk in buffer A (mM): Tris–HCl (pH 7.4), 12; NaCl, 160 and 0.1% Triton X-100 for 1 h at RT. After incubation with primary antibodies overnight at 4°C, the membranes were further incubated with horseradish peroxidase-coupled secondary antibodies (Biorad, 1:2000) for 1 h at RT. Bound peroxidase was detected using the ECL western-blotting reagents (Amersham). SDS–PAGE on non-reducing gels was performed on different samples as described earlier (Newby *et al*, 2002). For Co-IPs, cell lysates were pre-cleared for 2 h using superparamagnetic beads conjugated with recombinant protein A (Ademtech) before incubation with antibodies against PC1 (7e12), PC2 (p30, N-PC2 and G20, Santa Cruz Biotechnology), CD8 (Santa Cruz Biotechnology), c-myc (9e10, Serotec), Thio (Invitrogen), His (Abcam) FLAG, HA and Pk (Ong *et al*, 1999a, b) in 500 μl at 4°C for 1 h.

Confocal microscopy

Confocal image acquisition was performed using a Leica TCS SP2 laser scanning microscope equipped with 63 × /1.32 n.a. oil immersion lense. Images were obtained using the 488-nm band of an Argon laser and the 543-nm band of an He–Ne laser for excitation of FITC and TRITC, respectively. Spectral detection of emitted fluorescence was set as follows: 500–535 nm for FITC and 550–700 nm for TRITC. Dapi was excited at 780 nm using a Mira Verdi pulsed laser (Coherent). Emitted fluorescence was collected from 400 to 480 nm. Images were collected automatically as frame-by-frame sequential series, each image being produced from an average of three frame scans. The pinhole was adjusted to the first Airy. 3D-stacks of confocal images were acquired using a 0.5-μm step.

Electron microscopy

For ultrastructure analysis, cells expressing hPKD2 plasmids were fixed in 2% glutaraldehyde in 0.1 M sodium phosphate buffer, pH 7.3, and postfixed in osmium tetroxide vapour. Cells were dehydrated in graded alcohol solutions and embedded in SPURR low-viscosity medium. Ultrathin sections (50–60 nm) were counterstained with uranyl acetate and lead citrate before observation with a Philips CM10 TEM equipped with a digital camera (Advanced Microscopy Techniques). Immunoelectron microscopy was performed on cells that were cryosubstituted in a Reichert AFS freeze substitution (Leica) and embedded in Lowicryl HM20 for 2 days at −40°C. The ultrathin (90 nm) Lowicryl sections were pre-incubated with TBS containing 0.5% BSA. The sections were then incubated overnight at 4°C with rabbit N-PC2 (1:100) or mouse anti-HA (1:200) antibodies in TBS containing 0.05% Tween 20 and 0.1% BSA. Primary antibodies were visualized using goat anti-rabbit or anti-mouse IgG conjugated to 1 nm colloidal gold particles (1:30, for 1 h in TBS 0.1% BSA). The ultrathin Lowicryl sections were examined using a MET Zeiss EM 912 and a camera Gatan Bioscan 792. Immunolabelling controls were made by omitting primary antibodies. All controls showed absence of labelling.

Immunoprecipitation assays, cross-linking assay and recombinant protein preparation, GST and MBP pull-down assays, analytical ultracentrifugation and 2D NMR spectroscopy are described in the Supplementary data section.

Zebrafish MO, mRNA injections and RT–PCR

All injections were performed at the one cell stage. Control MO, *pkd2ATGMO* (Gene Tools, LLC) (Sun *et al*, 2004) and all the other *hPKD2* capRNAs are injected as described (Obara *et al*, 2006; Streets *et al*, 2006; Feng *et al*, 2008). *In vitro* transcribed capRNA coding *hPKD2*, *hPKD2-M849P* and *hPKD2-4M* were synthesized using a mMessage mMachine T7 kit (Ambion) and 50 pg mRNA was injected for *hPKD2* and *hPKD2-M849P* and 20 pg was injected for *hPKD2-4M*. These amounts of capRNA were chosen to optimize their effects on pronephric cyst formation. Histological analysis was performed at 48 h post fertilization (hpf) as described (Feng *et al*, 2008). Total RNA was isolated from 48 hpf zebrafish larvae by using RNAqueous® kit (Ambion). Nested RT–PCR primers were designed to only detect *hPKD2*, which express in zebrafish larvae. The hPKD2-specific primers used were: 2162F1: CCGTGGAATGACATTT CAGAGAG, 2902R1: CGTGGACATTAGAACTCCCATTT, 2174F2: TTT CAGAGAGTCTGCGGCAAG, 2873R2: GCACCTTCCATGCCTTCTGT AG. Amplification of zebrafish β-*actin* was performed as described before (Obara *et al*, 2006). RT–PCR was performed using the SuperScript III One-Step RT–PCR System with Platinum® Taq High Fidelity (Invitrogen) followed by a second PCR using Phusion High-Fidelity DNA Polymerase (New England BioLabs) according to the manufacture's protocols.

Statistical analysis

Data were expressed as the mean ± s.e.m. ANOVA and Student's *t* test were applied to determine the statistical significance and differences were considered significant if $P<0.05$.

Supplementary data

Supplementary data are available at The EMBO Journal Online (http://www.embojournal.org).

Acknowledgements

We thank the members of the Delmas and Ong laboratories for critical input, AJ Baron and J Courrageot for assistance with the AUC experiments and EM, respectively; Stanislaw Dunin-Horkawicz for the CC model, Jean-Paul Chauvin and Fabrice Richard from the Electron Microscopy facilities of IBDM for EM immunogold assays and François Maingret for designing Supplementary Figure 10. This study was supported by the French Ministry and the CNRS and by grants from the ANR, FRM, Fondation Schlumberger, ARCInca, UPSA and IRME (to PD), by the Wellcome Trust (GR071201) (to ACMO), by NIH Grants R21-DK069604, R01-DK078209 (to TO) and from the PKD foundation (69a2r) (to TO). AG was supported by a PhD studentship from the FRM, LR-D and CG were supported by a grant from the FRM, SF was supported by a PhD studentship from the Sheffield Area Kidney Association and YX by a University of Sheffield PhD scholarship.

Conflict of interest

The authors declare that they have no conflict of interest.

References

Anderson RG, Orci L, Brown MS, Garcia-Segura LM, Goldstein JL (1983) Ultrastructural analysis of crystalloid endoplasmic reticulum in UT-1 cells and its disappearance in response to cholesterol. *J Cell Sci* **63:** 1–20

Arnould T, Kim E, Tsiokas L, Jochimsen F, Gruning W, Chang JD, Walz G (1998) The polycystic kidney disease 1 gene product mediates protein kinase C alpha-dependent and c-Jun N-terminal kinase-dependent activation of the transcription factor AP-1. *J Biol Chem* **273:** 6013–6018

Bai CX, Giamarchi A, Rodat-Despoix L, Padilla F, Downs T, Tsiokas L, Delmas P (2008a) Formation of a new receptor-operated channel by heteromeric assembly of TRPP2 and TRPC1 subunits. *EMBO Rep* **9:** 472–479

Bai CX, Kim S, Li WP, Streets AJ, Ong AC, Tsiokas L (2008b) Activation of TRPP2 through mDia1-dependent voltage gating. *EMBO J* **27:** 1345–1356

Bhunia AK, Piontek K, Boletta A, Liu L, Qian F, Xu PN, Germino FJ, Germino GG (2002) PKD1 induces p21(waf1) and regulation of the cell cycle via direct activation of the JAK-STAT signaling pathway in a process requiring PKD2. *Cell* **109:** 157–168

Birnbaumer L, Boulay G, Brown D, Jiang M, Dietrich A, Mikoshiba K, Zhu X, Qin N (2000) Mechanism of capacitative Ca2 + entry (CCE): interaction between IP3 receptor and TRP links the internal calcium storage compartment to plasma membrane CCE channels. *Recent Prog Horm Res* **55:** 127–161; discussion 161–122

Bisgrove BW, Snarr BS, Emrazian A, Yost HJ (2005) Polaris and polycystin-2 in dorsal forerunner cells and Kupffer's vesicle are required for specification of the zebrafish left-right axis. *Dev Biol* **287:** 274–288

Cai Y, Maeda Y, Cedzich A, Torres VE, Wu G, Hayashi T, Mochizuki T, Park JH, Witzgall R, Somlo S (1999) Identification and characterization of polycystin-2, the PKD2 gene product. *J Biol Chem* **274:** 28557–28565

Calvet JP, Grantham JJ (2001) The genetics and physiology of polycystic kidney disease. *Semin Nephrol* **21:** 107–123

Celic A, Petri ET, Demeler B, Ehrlich BE, Boggon TJ (2008) Domain mapping of the polycystin-2 C-terminal tail using *de novo* molecular modeling and biophysical analysis. *J Biol Chem* **283:** 28305–28312

Damann N, Voets T, Nilius B (2008) TRPs in our senses. *Curr Biol* **18:** R880–R889

Delmas P (2004) Polycystins: from mechanosensation to gene regulation. *Cell* **118:** 145–148

Delmas P, Brown DA (2002) Junctional signaling microdomains: bridging the gap between the neuronal cell surface and Ca^{2+} stores. *Neuron* **36:** 787–790

Delmas P, Nauli SM, Li X, Coste B, Osorio N, Crest M, Brown DA, Zhou J (2004) Gating of the polycystin ion channel signaling complex in neurons and kidney cells. *FASEB J* **18:** 740–742

Delmas P, Nomura H, Li X, Lakkis M, Luo Y, Segal Y, Fernandez-Fernandez JM, Harris P, Frischauf AM, Brown DA, Zhou J (2002a) Constitutive activation of G-proteins by polycystin-1 is antagonized by polycystin-2. *J Biol Chem* **277:** 11276–11283

Delmas P, Wanaverbecq N, Abogadie FC, Mistry M, Brown DA (2002b) Signaling microdomains define the specificity of receptor-mediated InsP(3) pathways in neurons. *Neuron* **34:** 209–220

Deng Y, Liu J, Zheng Q, Eliezer D, Kallenbach NR, Lu M (2006) Antiparallel four-stranded coiled coil specified by a 3-3-1 hydrophobic heptad repeat. *Structure* **14:** 247–255

Feng S, Okenka GM, Bai CX, Streets AJ, Newby LJ, DeChant BT, Tsiokas L, Obara T, Ong AC (2008) Identification and functional characterization of an N-terminal oligomerization domain for polycystin-2. *J Biol Chem* **283:** 28471–28479

Foggensteiner L, Bevan AP, Thomas R, Coleman N, Boulter C, Bradley J, Ibraghimov-Beskrovnaya O, Klinger K, Sandford R (2000) Cellular and subcellular distribution of polycystin-2, the protein product of the PKD2 gene. *J Am Soc Nephrol* **11:** 814–827

Fu X, Wang Y, Schetle N, Gao H, Putz M, von Gersdorff G, Walz G, Kramer-Zucker AG (2008) The subcellular localization of TRPP2 modulates its function. *J Am Soc Nephrol* **19:** 1342–1351

Fujiwara Y, Minor Jr DL (2008) X-ray crystal structure of a TRPM assembly domain reveals an antiparallel four-stranded coiled-coil. *J Mol Biol* **383:** 854–870

Gabow PA (1990) Autosomal dominant polycystic kidney disease–more than a renal disease. *Am J Kidney Dis* **16:** 403–413

Geng L, Boehmerle W, Maeda Y, Okuhara DY, Tian X, Yu Z, Choe CU, Anyatonwu GI, Ehrlich BE, Somlo S (2008) Syntaxin 5 regulates the endoplasmic reticulum channel-release properties of polycystin-2. *Proc Natl Acad Sci USA* **105:** 15920–15925

Geng L, Okuhara D, Yu Z, Tian X, Cai Y, Shibazaki S, Somlo S (2006) Polycystin-2 traffics to cilia independently of polycystin-1 by using an N-terminal RVxP motif. *J Cell Sci* **119:** 1383–1395

Giamarchi A, Padilla F, Coste B, Raoux M, Crest M, Honore E, Delmas P (2006) The versatile nature of the calcium-permeable cation channel TRPP2. *EMBO Rep* **7:** 787–793

Gonzalez-Perrett S, Kim K, Ibarra C, Damiano AE, Zotta E, Batelli M, Harris PC, Reisin IL, Arnaout MA, Cantiello HF (2001) Polycystin-2, the protein mutated in autosomal dominant polycystic kidney disease (ADPKD), is a Ca2 + -permeable nonselective cation channel. *Proc Natl Acad Sci USA* **98:** 1182–1187

Hanaoka K, Qian F, Boletta A, Bhunia AK, Piontek K, Tsiokas L, Sukhatme VP, Guggino WB, Germino GG (2000) Co-assembly of polycystin-1 and -2 produces unique cation-permeable currents. *Nature* **408:** 990–994

Harris PC (1999) Autosomal dominant polycystic kidney disease: clues to pathogenesis. *Hum Mol Genet* **8:** 1861–1866

Hughes J, Ward CJ, Peral B, Aspinwall R, Clark K, San Millan JL, Gamble V, Harris PC (1995) The polycystic kidney disease 1 (PKD1) gene encodes a novel protein with multiple cell recognition domains. *Nat Genet* **10:** 151–160

Ishimaru Y, Inada H, Kubota M, Zhuang H, Tominaga M, Matsunami H (2006) Transient receptor potential family members PKD1L3 and PKD2L1 form a candidate sour taste receptor. *Proc Natl Acad Sci USA* **103:** 12569–12574

Jenke M, Sanchez A, Monje F, Stuhmer W, Weseloh RM, Pardo LA (2003) C-terminal domains implicated in the functional surface expression of potassium channels. *EMBO J* **22:** 395–403

Karcher C, Fischer A, Schweickert A, Bitzer E, Horie S, Witzgall R, Blum M (2005) Lack of a laterality phenotype in Pkd1 knock-out embryos correlates with absence of polycystin-1 in nodal cilia. *Differentiation* **73:** 425–432

Kim E, Arnould T, Sellin L, Benzing T, Comella N, Kocher O, Tsiokas L, Sukhatme VP, Walz G (1999) Interaction between RGS7 and polycystin. *Proc Natl Acad Sci USA* **96:** 6371–6376

Kim JY, Kim MK, Kang GB, Park CS, Eom SH (2008) Crystal structure of the leucine zipper domain of small-conductance Ca^{2+}-activated K^+ (SK(Ca)) channel from Rattus norvegicus. *Proteins* **70:** 568–571

Kobori T, Smith GD, Sandford R, Edwardson JM (2009) The transient receptor potential (TRP) channels TRPP2 and TRPC1 form a heterotetramer with a 2:2 stoichiometry and an alternating subunit arrangement. *J Biol Chem* **284:** 35507–35513

Köttgen M, Buchholz B, Garcia-Gonzalez MA, Kotsis F, Fu X, Doerken M, Boehlke C, Steffl D, Tauber R, Wegierski T, Nitschke R, Suzuki M, Kramer-Zucker A, Germino GG, Watnick T, Prenen J, Nilius B, Kuehn EW, Walz G (2008) TRPP2 and TRPV4 form a polymodal sensory channel complex. *J Cell Biol* **182:** 437–447

Köttgen M, Walz G (2005) Subcellular localization and trafficking of polycystins. *Pflugers Arch* **451:** 286–293

Koulen P, Cai Y, Geng L, Maeda Y, Nishimura S, Witzgall R, Ehrlich BE, Somlo S (2002) Polycystin-2 is an intracellular calcium release channel. *Nat Cell Biol* **4:** 191–197

Li Q, Montalbetti N, Wu Y, Ramos A, Raychowdhury MK, Chen XZ, Cantiello HF (2006) Polycystin-2 cation channel function is under the control of microtubular structures in primary cilia of renal epithelial cells. *J Biol Chem* **281:** 37566–37575

Li Y, Wright JM, Qian F, Germino GG, Guggino WB (2005) Polycystin 2 interacts with type I inositol 1,4,5-trisphosphate receptor to modulate intracellular Ca2 + signaling. *J Biol Chem* **280:** 41298–41306

LopezJimenez ND, Cavenagh MM, Sainz E, Cruz-Ithier MA, Battey JF, Sullivan SL (2006) Two members of the TRPP family of ion channels, Pkd1l3 and Pkd2l1, are co-expressed in a subset of taste receptor cells. *J Neurochem* **98:** 68–77

Ludwig J, Owen D, Pongs O (1997) Carboxy-terminal domain mediates assembly of the voltage-gated rat ether-a-go-go potassium channel. *EMBO J* **16:** 6337–6345

Luik RM, Wang B, Prakriya M, Wu MM, Lewis RS (2008) Oligomerization of STIM1 couples ER calcium depletion to CRAC channel activation. *Nature* **454:** 538–542

Luo Y, Vassilev PM, Li X, Kawanabe Y, Zhou J (2003) Native polycystin 2 functions as a plasma membrane Ca2 + -permeable cation channel in renal epithelia. *Mol Cell Biol* **23:** 2600–2607

Lupas A, Van Dyke M, Stock J (1991) Predicting coiled coils from protein sequences. *Science* **252:** 1162–1164

Ma R, Li WP, Rundle D, Kong J, Akbarali HI, Tsiokas L (2005) PKD2 functions as an epidermal growth factor-activated plasma membrane channel. *Mol Cell Biol* **25:** 8285–8298

McGrath J, Somlo S, Makova S, Tian X, Brueckner M (2003) Two populations of node monocilia initiate left-right asymmetry in the mouse. *Cell* **114:** 61–73

Mochizuki T, Wu G, Hayashi T, Xenophontos SL, Veldhuisen B, Saris JJ, Reynolds DM, Cai Y, Gabow PA, Pierides A, Kimberling WJ, Breuning MH, Deltas CC, Peters DJ, Somlo S (1996) PKD2, a gene for polycystic kidney disease that encodes an integral membrane protein. *Science* **272:** 1339–1342

Nauli SM, Alenghat FJ, Luo Y, Williams E, Vassilev P, Li X, Elia AE, Lu W, Brown EM, Quinn SJ, Ingber DE, Zhou J (2003) Polycystins 1 and 2 mediate mechanosensation in the primary cilium of kidney cells. *Nat Genet* **33:** 129–137

Newby LJ, Streets AJ, Zhao Y, Harris PC, Ward CJ, Ong AC (2002) Identification, characterization, and localization of a novel kidney polycystin-1-polycystin-2 complex. *J Biol Chem* **277:** 20763–20773

Obara T, Mangos S, Liu Y, Zhao J, Wiessner S, Kramer-Zucker AG, Olale F, Schier AF, Drummond IA (2006) Polycystin-2 immunolocalization and function in zebrafish. *J Am Soc Nephrol* **17:** 2706–2718

Ong AC, Harris PC (2005) Molecular pathogenesis of ADPKD: the polycystin complex gets complex. *Kidney Int* **67:** 1234–1247

Ong AC, Harris PC, Davies DR, Pritchard L, Rossetti S, Biddolph S, Vaux DJ, Migone N, Ward CJ (1999a) Polycystin-1 expression in PKD1, early-onset PKD1, and TSC2/PKD1 cystic tissue. *Kidney Int* **56:** 1324–1333

Ong AC, Ward CJ, Butler RJ, Biddolph S, Bowker C, Torra R, Pei Y, Harris PC (1999b) Coordinate expression of the autosomal dominant polycystic kidney disease proteins, polycystin-2 and polycystin-1, in normal and cystic tissue. *Am J Pathol* **154:** 1721–1729

Parnell SC, Magenheimer BS, Maser RL, Zien CA, Frischauf AM, Calvet JP (2002) Polycystin-1 activation of c-Jun N-terminal kinase and AP-1 is mediated by heterotrimeric G proteins. *J Biol Chem* **277:** 19566–19572

Pennekamp P, Karcher C, Fischer A, Schweickert A, Skryabin B, Horst J, Blum M, Dworniczak B (2002) The ion channel polycystin-2 is required for left-right axis determination in mice. *Curr Biol* **12:** 938–943

Phelps CB, Gaudet R (2007) The role of the N terminus and transmembrane domain of TRPM8 in channel localization and tetramerization. *J Biol Chem* **282:** 36474–36480

Praetorius HA, Spring KR (2003) Removal of the MDCK cell primary cilium abolishes flow sensing. *J Membr Biol* **191:** 69–76

Qian F, Germino FJ, Cai Y, Zhang X, Somlo S, Germino GG (1997) PKD1 interacts with PKD2 through a probable coiled-coil domain. *Nat Genet* **16:** 179–183

Roitbak T, Surviladze Z, Tikkanen R, Wandinger-Ness A (2005) A polycystin multiprotein complex constitutes a cholesterol-containing signalling microdomain in human kidney epithelia. *Biochem J* **392:** 29–38

Rossetti S, Consugar MB, Chapman AB, Torres VE, Guay-Woodford LM, Grantham JJ, Bennett WM, Meyers CM, Walker DL, Bae K, Zhang QJ, Thompson PA, Miller JP, Harris PC (2007) Comprehensive molecular diagnostics in autosomal dominant polycystic kidney disease. *J Am Soc Nephrol* **18:** 2143–2160

Sandford R, Sgotto B, Aparicio S, Brenner S, Vaudin M, Wilson RK, Chissoe S, Pepin K, Bateman A, Chothia C, Hughes J, Harris P (1997) Comparative analysis of the polycystic kidney disease 1 (PKD1) gene reveals an integral membrane glycoprotein with multiple evolutionary conserved domains. *Hum Mol Genet* **6:** 1483–1489

Scheffers MS, Le H, van der Bent P, Leonhard W, Prins F, Spruit L, Breuning MH, de Heer E, Peters DJ (2002) Distinct subcellular expression of endogenous polycystin-2 in the plasma membrane and Golgi apparatus of MDCK cells. *Hum Mol Genet* **11:** 59–67

Schmitt N, Schwarz M, Peretz A, Abitbol I, Attali B, Pongs O (2000) A recessive C-terminal Jervell and Lange-Nielsen mutation of the KCNQ1 channel impairs subunit assembly. *EMBO J* **19:** 332–340

Schottenfeld J, Sullivan-Brown J, Burdine RD (2007) Zebrafish curly up encodes a Pkd2 ortholog that restricts left-side-specific expression of southpaw. *Development* **134:** 1605–1615

Schwake M, Jentsch TJ, Friedrich T (2003) A carboxy-terminal domain determines the subunit specificity of KCNQ K+ channel assembly. *EMBO Rep* **4:** 76–81

Sharif-Naeini R, Folgering JH, Bichet D, Duprat F, Lauritzen I, Arhatte M, Jodar M, Dedman A, Chatelain FC, Schulte U, Retailleau K, Loufrani L, Patel A, Sachs F, Delmas P, Peters DJ, Honoré E (2009) Polycystin-1 and -2 dosage regulates pressure sensing. *Cell* **139:** 587–596

Streets AJ, Moon DJ, Kane ME, Obara T, Ong AC (2006) Identification of an N-terminal glycogen synthase kinase 3 phosphorylation site which regulates the functional localization of polycystin-2 *in vivo* and *in vitro*. *Hum Mol Genet* **15:** 1465–1473

Streets AJ, Wagner BE, Harris PC, Ward CJ, Ong AC (2009) Homophilic and heterophilic polycystin 1 interactions regulate E-cadherin recruitment and junction assembly in MDCK cells. *J Cell Sci* **122:** 1410–1417

Sullivan-Brown J, Schottenfeld J, Okabe N, Hostetter CL, Serluca FC, Thiberge SY, Burdine RD (2008) Zebrafish mutations affecting cilia motility share similar cystic phenotypes and suggest a mechanism of cyst formation that differs from pkd2 morphants. *Dev Biol* **314:** 261–275

Sun Z, Amsterdam A, Pazour GJ, Cole DG, Miller MS, Hopkins N (2004) A genetic screen in zebrafish identifies cilia genes as a principal cause of cystic kidney. *Development* **131:** 4085–4093

Takei K, Mignery GA, Mugnaini E, Sudhof TC, De Camilli P (1994) Inositol 1,4,5-trisphosphate receptor causes formation of ER cisternal stacks in transfected fibroblasts and in cerebellar Purkinje cells. *Neuron* **12:** 327–342

Tsiokas L, Arnould T, Zhu C, Kim E, Walz G, Sukhatme VP (1999) Specific association of the gene product of PKD2 with the TRPC1 channel. *Proc Natl Acad Sci USA* **96:** 3934–3939

Tsiokas L, Kim E, Arnould T, Sukhatme VP, Walz G (1997) Homo- and heterodimeric interactions between the gene products of PKD1 and PKD2. *Proc Natl Acad Sci USA* **94:** 6965–6970

Tsuruda PR, Julius D, Minor Jr DL (2006) Coiled coils direct assembly of a cold-activated TRP channel. *Neuron* **51:** 201–212

Wessely O, Obara T (2008) Fish and frogs: models for vertebrate cilia signaling. *Front Biosci* **13:** 1866–1880

Wiener R, Haitin Y, Shamgar L, Fernández-Alonso MC, Martos A, Chomsky-Hecht O, Rivas G, Attali B, Hirsch JA (2008) The KCNQ1 (Kv7.1) COOH terminus, a multitiered scaffold for subunit assembly and protein interaction. *J Biol Chem* **283:** 5815–5830

Wright R, Keller G, Gould SJ, Subramani S, Rine J (1990) Cell-type control of membrane biogenesis induced by HMG-CoA reductase. *New Biol* **2:** 915–921

Wu G, Somlo S (2000) Molecular genetics and mechanism of autosomal dominant polycystic kidney disease. *Mol Genet Metab* **69:** 1–15

Wu Y, Dai XQ, Li Q, Chen CX, Mai W, Hussain Z, Long W, Montalbetti N, Li G, Glynne R, Wang S, Cantiello HF, Wu G, Chen XZ (2006) Kinesin-2 mediates physical and functional interactions between polycystin-2 and fibrocystin. *Hum Mol Genet* **15:** 3280–3292

Xu Q, Minor Jr DL (2009) Crystal structure of a trimeric form of the K(V)7.1 (KCNQ1) a-domain tail coiled-coil reveals structural plasticity and context dependent changes in a putative coiled-coil trimerization motif. *Protein Sci* **18:** 2100–2114, PubMed PMID: 19693805

Yoder BK, Hou X, Guay-Woodford LM (2002) The polycystic kidney disease proteins, polycystin-1, polycystin-2, polaris, and cystin, are co-localized in renal cilia. *J Am Soc Nephrol* **13:** 2508–2516

Yu Y, Ulbrich MH, Li MH, Buraei Z, Chen XZ, Ong AC, Tong L, Isacoff EY, Yang J (2009) Structural and molecular basis of the assembly of the TRPP2/PKD1 complex. *Proc Natl Acad Sci USA* **106:** 11558–11563

Zhang P, Luo Y, Chasan B, Gonzalez-Perrett S, Montalbetti N, Timpanaro GA, Cantero Mdel R, Ramos AJ, Goldmann WH, Zhou J, Cantiello HF (2009) The multimeric structure of polycystin-2 (TRPP2): structural-functional correlates of homo- and hetero-multimers with TRPC1. *Hum Mol Genet* **18:** 1238–1251